SEASONAL VARIABILITY OF TOTAL SUSPENDED MATTER IN MINAS BASIN, BAY OF FUNDY

by

Jing Tao

Submitted in partial fulfilment of the requirements
for the degree of Master of Science

at

Dalhousie University
Halifax, Nova Scotia
July 2013

For my parents, who encouraged me all the way long.
I love them forever.

TABLE OF CONTENTS

LIST OF TABLES v
LIST OF FIGURES vi
ABSTRACT viii
LIST OF ABBREVIATIONS AND SYMBOLS USED ix
ACKNOWLEDGEMENTS xi
CHAPTER 1 INTRODUCTION 1
1.1 Background 1
1.2 Geology of Minas Basin 2
1.3 Literature Review 4
1.3.1 Point Measurements 4
1.3.2 Satellite Measurements 5
1.3.3 Numerical Modelling 7
1.4 Objectives 9
1.5 Structure of Thesis 9
CHAPTER 2 MATERIALS AND METHODOLOGY 10
2.1 Materials 10
2.1.1 MERIS Satellite 10
2.1.2 *In situ* Data 14
2.1.3 Delft3D Model Set-up 18
2.2 Methodology 26
2.2.1 Autocorrelation Analysis 26
2.2.2 Relative Difference 27
CHAPTER 3 RESULTS 29
3.1 Satellite TSM Concentration 29
3.1.1 Time Series and Sample Variogram of Satellite TSM Concentration 29
3.1.2 Seasonal Variability of Satellite TSM Concentration 34
3.2 Strength of Annual Signal 38
3.3 Delft3D Model 38
3.3.1 Delft3D Hydrodynamics 38
3.3.2 Delft3D Sediment Dynamics 39

3.4 Satellite versus Model TSM Concentration 43
CHAPTER 4 DISCUSSION 49
4.1 Strong Annual Signal 49
4.1.1 Comparison of satellite-derived and *in situ* TSM Concentration 49
4.1.2 Causes for Annual Cycle of TSM Concentration 51
4.2 Accuracy of Satellite-Derived vs. Modelled TSM in Shallow Regions 52
4.2.1 Accuracy of Satellite MERIS TSM Concentration 53
4.2.2 Accuracy of Delft3D TSM Concentration 54
4.2.3 Accuracy of Comparison 55
CHAPTER 5 CONCLUSION AND RECOMMENDATIONS 57
5.1 Summary of Scientific Results 57
5.2 Recommendations 58
BIBLIOGRAPHY 59
APPENDIX A MERIS SPECTRAL BANDS AND APPLICATIONS 63
APPENDIX B DELFT3D MEAN TSM CONCENTRATION IN MINAS BASIN 64
APPENDIX C SATELLITE AND MODEL COMPARISONS 68

LIST OF TABLES

Table 1: The location, period of observation and tidal characteristics of the stations occupied during a survey of the water quality in Minas Basin. 16

Table 2: The mean and standard deviation of surficial TSM (0 - 1 m) for various dates in 1975-76 at Amos and Joyce (1977) sites in Minas Basin. 17

Table 3: The TSM profile collected at Location A5 on March 2012. 17

Table 4: Summary of Delft3D model sediment input parameters for each run. 25

Table 5: Summary of site locations and TSM concentration in Minas Basin. 33

Table 6: List of Delft3D model processing parameters and corresponding green ratio for each run. 47

Table 7: TSM comparisons between MERIS satellite and *in situ* surface measurements at A5 in March and April. 51

LIST OF FIGURES

Figure 1: Map of Minas Basin, Nova Scotia, Canada..... 1

Figure 2: Observed distribution of bottom sediment in Minas Basin..... 3

Figure 3: Thematic map of TSM in Minas Basin derived from chromaticity analysis of Landsat digital data 1430 GMT, May 3, 1974 7

Figure 4: Concentrations of total suspended matter (TSM; g/m^3) derived from a MERIS image in the upper Bay of Fundy on 1506 GMT, February 10th, 2010. 13

Figure 5: Time series of mean values of TSM over a 3×3 pixel box surrounding the A5 13

Figure 6: Comparison of TSM concentrations of MERIS and *in-situ* observations within the Northumberland Strait on October 17th, 2006..... 14

Figure 7: Sites of suspended sediment survey in Minas Basin. 15

Figure 8: Governing parameters for sedimentation and re-suspension of sediment..... 22

Figure 9: Delft3D-FLOW model domain of Minas Basin in m..... 24

Figure 10: Location map of the intertidal zone in Minas Basin – Cobequid Bay area..... 25

Figure 11: Positions of four sites in Minas Basin, at which TSM concentration time series are used in analyses. 30

Figure 12: Time series of TSM concentration derived from the MERIS satellite: a) mean values of TSM concentration over a 1 km^2 pixel box (3×3 pixels) at MB in the centre of Minas Basin from May 2008 to July 2011; b) sample variograms of TSM at same location. 31

Figure 13: Time series of a) TSM concentration derived from the MERIS satellite and b) variogram calculated from the time series at site WB. 32

Figure 14: Time series of a) TSM concentration derived from the MERIS satellite and b) variogram calculated from the time series at site BH. 32

Figure 15: Time series of a) TSM concentration derived from the MERIS satellite and b) variogram calculated from the time series at site CB. 33

Figure 16: Distributions of time-averaged satellite-derived mean TSM concentration estimated from MERIS images during a) Summer and b) Winter 2009 in Minas Basin. 35

Figure 17: Distributions of maximum satellite-derived TSM concentration estimated from MERIS images during a) Summer and b) Winter 2009 in Minas Basin. . 36

Figure 18: Satellite TSM concentration seasonal differences between summer and winter, normalized by winter values, in 2009 in Minas Basin. 37

Figure 19: Distributions of estimated annual change in TSM concentration observed by the MERIS satellite. 38

Figure 20: Comparison of observed horizontal current velocity components (u, v) and speed (s) time series at the 11 m depth at site A5. 39

Figure 21: Runs showing the a) maximum and b) minimum amount of TSM concentration simulated by Delft3D with given parameters. 41

Figure 22: The time-mean concentration of sediment mud simulated by Delft3D model with optimal parameters in Minas Basin. 42

Figure 23: Quantitative comparison between model and satellite-derived TSM concentration during summer 2010 45

Figure 24: Quantitative comparison between model and satellite-derived TSM concentration during winter 2009. 46

Figure 25: Seasonal variability of Delft3D model TSM concentration in Minas Basin (Runs 310 and 311). 48

Figure 26: Comparison between *in situ* TSM, satellite-derived TSM and Max. satellite-derived TSM at several sites in Minas Basin 50

Figure 27: TSM concentrationcomparison between satellite-derived (2010) and *in situ* (1975-76) measurements at Amos and Joyce (1977) sites in Minas Basin during summer 50

ABSTRACT

Total suspended matter (TSM) concentrations were derived from ocean colour imagery (MERIS data) in Minas Basin. Analysis of time series of TSM in 1-km^2 pixel boxes throughout the Basin revealed an annual cycle in TSM in most parts of the Basin. Higher TSM of up to 85 g/m^3 was observed in late-winter (February - March), and lower TSM of 5-10 g/m^3 characterized late-summer (July - August). The largest annual variation occurred in the centre of Basin, and the smallest variation occurred in shallow areas. Satellite-derived TSM were compared to predictions using the Delft3D model. Increasing model erosion rate in winter relative to summer was necessary to improve agreement between model and satellite-derived TSM. In comparison with the satellite-derived estimates, the model underestimated TSM in shallow areas in summer and overestimated it in winter. This discrepancy is likely due to inaccurate satellite-derived TSM in shallow, high concentration areas of the Basin.

LIST OF ABBREVIATIONS AND SYMBOLS USED

ADCP	Acoustic Doppler Current Profilers
BH	Burntcoat Head
BIO	Bedford Institute of Oceanography
CB	Cobequid Bay
ERTS	Earth Resources Technology Satellite
ESA	European Space Agency
FR	Full Resolution
FVCOM	Finite Volume Coastal Ocean Model
IDL	Interface Description Language
IOP	Inherent Optical Properties
MATLAB	MATrix LABoratory
MB	Minas Basin
MERIS	Medium Resolution Imaging Spectrometer
MODIS	Moderate Resolution Imaging Spectroradiometer
NSERC	Natural Sciences and Engineering Research Council of Canada
OEER	Offshore Energy Environmental Research Association
OETR	Offshore Energy Technical Research Association
RD	Relative Differences
RR	Reduced Resolution
SD	Standard Deviation
SeaDAS	SeaWiFS Data Analysis System
SeaWiFS	Sea-viewing Wide Field-of-view Sensor
TSM	Total Suspended Matter
WB	Windsor Bay

Symbol	Description	Unites
x	eastward coordinate	m
y	northward coordinate	m
z	upward coordinate	m
t	time	s, hr, d
c	mass concentration of sediment	kg m^{-3}
u	flow velocity component in x direction	m s^{-1}
v	flow velocity component in y direction	m s^{-1}
w	flow velocity component in z direction	m s^{-1}
$\varepsilon_{s,x}$	eddy diffusivities in x direction	m^2 s^{-1}
$\varepsilon_{s,y}$	eddy diffusivities in y direction	m^2 s^{-1}
$\varepsilon_{s,z}$	eddy diffusivities in z direction	m^2 s^{-1}
w_s	settling velocity of suspended sediment	m s^{-1}
ζ	sea surface elevation	m
D	deposition flux of suspended matter	kg m^{-2} s^{-1}
E	re-suspension flux	kg m^{-2} s^{-1}
z_b	the location of the bed	m
M	erosion parameter	kg m^{-2} s^{-1}
τ_{cw}	bed shear stress due to current and waves	N m^{-2}
τ_{e_crit}	critical bed shear stress for erosion	N m^{-2}
τ_{d_crit}	critical bed shear stress for deposition	N m^{-2}
c_b	average sediment concentration in the near bottom computational layer	kg m^{-3}
s	speed	m s^{-1}
k	time lag	day
$E(x)$	expected values of x	-
$y(\mathrm{t})$	a stationary random process	-
$V(k)$	variogram	-
σ^2	variance	-
$\mathrm{V_v(k)}$	normalized sample variogram	-

ACKNOWLEDGEMENTS

Many individuals helped me during my thesis work. It is my esteemed pleasure to acknowledge the help of my Supervisor Dr. Paul S. Hill who assisted me to complete this project. His guidance during this thesis has been invaluable, and his enthusiasm for the project was inspiring. I would like to thank my co-supervisor Dr. Ryan P. Mulligan from Queen's University, who gave me guidance for the Delft3D-FLOW model and provided the results of the Delft3D in this study. I also would like to thank the other committee members, Dr. Jinyu Sheng (Dalhousie University) and Dr. Peter C. Smith (Bedford Institute of Oceanography), for their committed support to me for finishing this project. MERIS satellite data were kindly provided by Carla Caverhill and Cathy Porter from Bedford Institute of Oceanography (BIO). I also thank members of our particle group at Dalhousie University for their useful suggestions. The faculty, staff, and students are thanked for giving me the skills and the motivation to pursue oceanography. I gratefully acknowledge funding from Offshore Energy Environmental Research Association (OEER), Offshore Energy Technical Research Association (OETR), Natural Sciences and Engineering Research Council of Canada (NSERC) and Dalhousie University. Special thanks go out to my parents whom I love dearly for their unremitting support and confidence.

Jing Tao

CHAPTER 1 INTRODUCTION

1.1 Background

The Bay of Fundy is a large macro-tidal embayment situated on the east coast of Canada between the provinces of New Brunswick and Nova Scotia. It is characterized by a semi-diurnal tidal regime with a maximum tidal range of 16.3 m and high suspended sediment concentrations (van Proosdij *et al.,* 2009). The Chignecto Bay system forms the northern upper reaches of the Bay of Fundy, and it is subdivided into Chignecto Bay, Shepody Bay and Cumberland Basin. The Minas Basin system extends off the central Bay to the east, and it has been divided into three regions: Minas Channel, Minas Basin and Cobequid Bay (Figure 1). Minas Channel lies west of Minas Passage. Minas Passage lies between Cape Split and the Parrsboro shore and it is a narrow waterway connecting Minas Channel to Minas Basin. The seafloor of Minas Basin is dominated by large accumulations of sand.

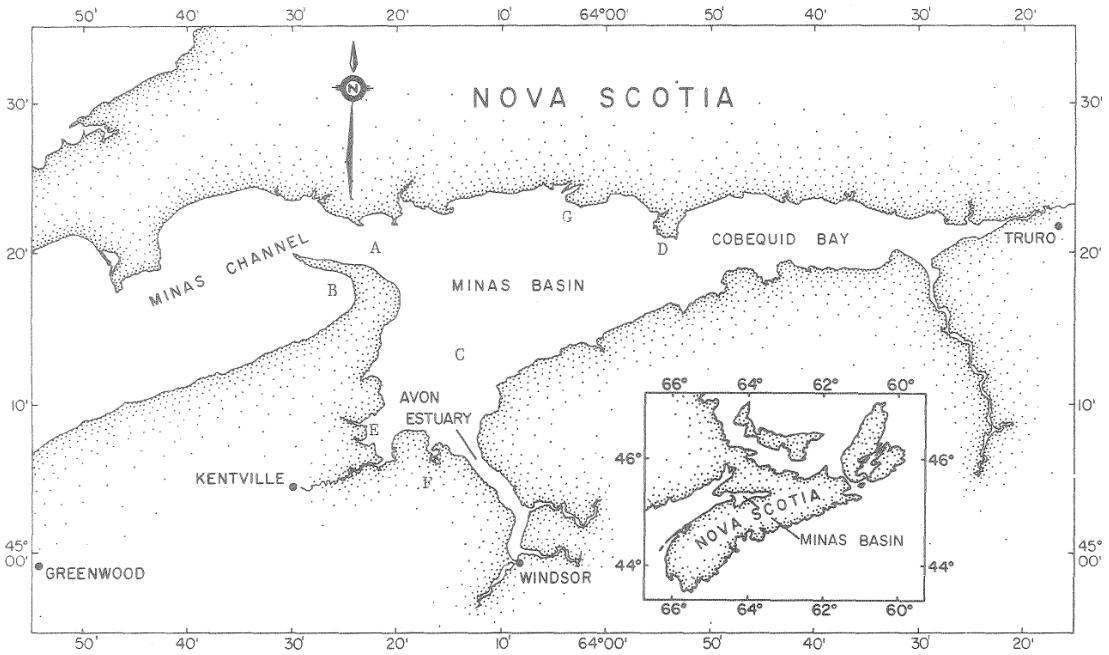

Figure 1: Map of Minas Basin, Nova Scotia, Canada. A-Minas Passage, B-Scot's Bay, C-Windsor Bay, D-Economy Point, E-Cornwallis Estuary, F-Gaspereau Estuary, G-Five Islands (Amos and Joice, 1977).

The physical environment in the Bay of Fundy is dominated by storm waves and tidal currents (Fader *et al.*, 1977). The strong current through Minas Passage is an attractive target for the generation of electrical power using in-stream turbines. The energy in the tides is also fundamental to the environment and ecology in the Bay of Fundy. Significant extraction of tidal energy from this system could lead to local and far field changes in the tidal regime. For example, in-stream turbines to be deployed in Minas Basin could impose changes to the oceanographic conditions on the tidal flats, at the shoreline, and in river channels in the Basin that might result in additional sediment erosion/accretion as the system adjusts to a new equilibrium.

Distribution of suspended sediments in the tidal regions of the Basin varies considerably with the stage of the tide. High tidal current velocities maintain high turbidity levels in Minas Basin (Dadswell *et al.,* 1986) and thereby keep fine-grained sediment continually in suspension. Extraction of energy from the tidal currents may cause a decrease in the suspended sediment concentration in the Basin.

In coastal and estuarine environments, total suspended matter (TSM) plays a significant role in physical, biological, and chemical processes (Miller *et al.,* 2011). A unique feature of Minas Basin is that biological community structure and trophic pathways seem to be controlled by dynamics of suspended sediment. For example, because Minas Basin is an area of high turbidity, primary production is hampered, and high densities of suspension and deposit feeding organisms are found in the region (Daborn, 1984). Understanding of the seasonal dynamics of TSM in the Basin is vital to understanding the entire ecosystem.

1.2 Geology of Minas Basin

The embayment in Minas Basin has the highest recorded tides in the world. The associated tidal current exceeds 300 cm/s, which is observed over the area where Minas Basin connects to Minas Passage. The tidal currents in the Passage are even higher.

Minas Basin system is 77 km long and up to 31 km wide (Amos, 1979). The resident suspended sediment volume in Minas Basin was calculated to be $30x10^6$ m^3 (Greenberg and Amos, 1983). The previous studies that have identified sources, sinks and transport of sediment determined that Minas Basin is a "sand-particle" basin in contrast to Chignecto Bay (a "muddy estuary"). The abundance of sand in Minas Basin is the result of erosion of Triassic sandstone cliffs that surround the shoreline, supplemented by the input of glacial outwash sand (Thomas, 1976; Stea, 2003). Sand is not the only sediment type in the Basin (Figure 2). Within the northern part of Minas Basin, the associated tidal channels are composed of gravelly sand, sand and gravel, and gravels. The percentage of sand also decreases south of Economy Point. Muds accumulate predominantly in sheltered embayments and within the upper intertidal zone surrounding Minas Basin (Greenberg and Amos, 1983). The area of the tidal flats in Minas Basin is about 35,800 ha in extent, almost half of it in Cobequid Bay. The TSM in Cobequid Bay is much higher than that in the Bay's tributary rivers above any tidal influence. The large amount of suspended sediment in the water is probably related to the re-suspension of mud from intertidal mudflats through wave and current activity. Knight (1980) describes this sediment as mostly silt- and clay-sized particles, not sand-sized sediments (Parker *et al*., 2007).

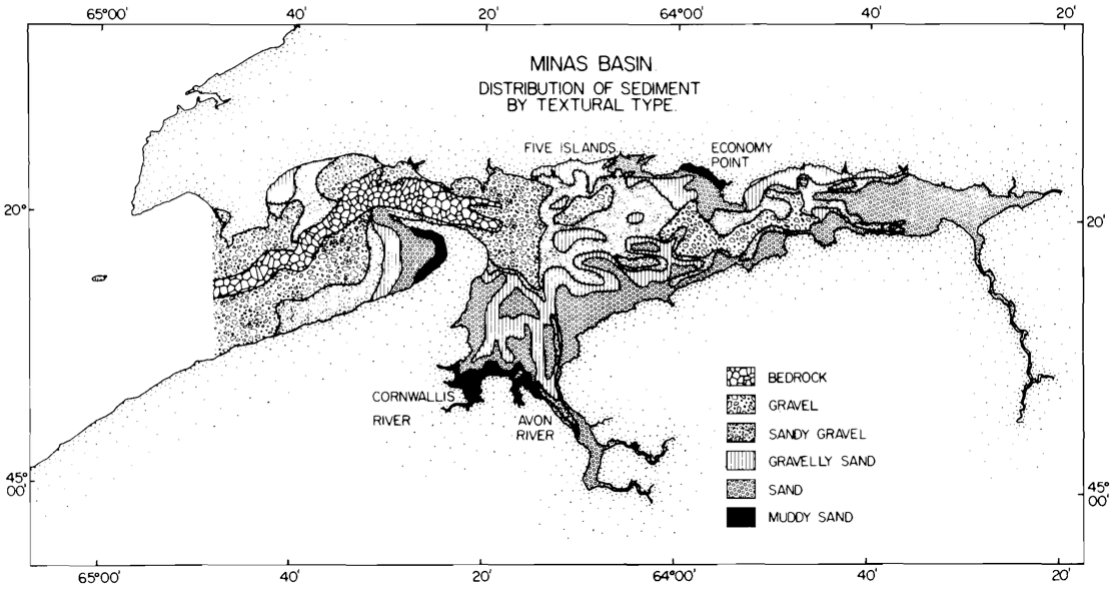

Figure 2: Observed distribution of bottom sediment in Minas Basin (Greenberg and Amos, 1983).

1.3 Literature Review

The temporal-spatial distribution of TSM in the Bay of Fundy is complicated and strongly affected by currents, waves and wind-driven re-suspension of bottom sediments (Dalrymple *et al*., 1990). Three general methods have been developed to understand sediment dynamics in the study area. Traditional sampling techniques (such as water bottles or pumps), although relatively accurate, are labor-intensive and inherently under-sample in terms of spatial and temporal resolution (Gray and Gartner, 2009). Several remote sensing techniques were developed in order to understand the processes of sedimentation and re-suspension over large spatial and temporal scales (Shen *et al*., 2010a). Numerical modelling of sediment transport has been recognized as a valuable tool for understanding and predicting morphological developments (Amos and Mosher, 1985). A brief summary of *in situ*, remote sensing and numerical modelling works for the study area is described in this section.

1.3.1 Point Measurements

In situ observations of TSM made in Minas Basin include collection of water samples and sediment samples from moorings and cruise surveys. *In situ* current velocity measurements were made by ADCPs (Acoustic Doppler Current Profilers) at various locations in the Basin for examining the currents and transport of suspended sediment.

The large exchange of water with each tide keeps a large amount of fine-grained sediment in suspension in Minas Basin. Knight (1977) found that TSM concentrations (based on 77 water samples) varied during the tidal cycle, ranging from 70 to over 2700 mg/l in Cobequid Bay. The highest concentrations occur during the late ebb and early flood when water depths are relatively shallow and shortly after the time of the maximum ebb and flood current velocities. The TSM concentration in the main Bay of Fundy ranges from 0.2 to 30.4 mg/l with an average of 6.6 mg/l, and concentration ranges from approximately 20 mg/l to 200 mg/l in Minas Basin (Amos, 1979). It is noted that the two units are equal: mg/l and g/m^3 in this thesis. The historical results demonstrate the general

variation of TSM in Minas Basin. There is a consistent increase in the suspended sediment concentration from Minas Passage into Cobequid Bay and Windsor Bay, and the concentration is generally higher along the southern shoreline of Minas Basin. The highest concentrations are found in Cobequid Bay, in the Avon river estuary, and over the intertidal zone (Amos, 1979). Furthermore, the suspended sediment concentration is the highest at low water levels and decreases at high water (Parker *et al*., 2007).

The advantages of *in situ* observations are reduced uncertainty of TSM estimates, and ability to analyze other sediment properties. For example, sediment samples were analyzed for their mineral composition, organic content and particle size distribution (Shen *et al*., 2010b). Traditional measurements of TSM through *in situ* sampling are expensive and time-consuming to perform. Additionally, this method cannot provide continuous TSM records.

1.3.2 Satellite Measurements

Remote sensing from space provides a unique perspective of the TSM load in the near surface waters of shelf seas and estuaries. With the development of remote sensing technology, satellite estimates of water quality significantly complement conventional monitoring techniques and have found widespread applications. Ocean color observations from space can produce nearly daily synoptic views of the distribution of water substances and concentrations with large spatial and temporal coverage, which is not available from other sources (Shen *et al*., 2010a).

In previous research, Munday *et al*. (1979) showed a thematic map of TSM in Minas Basin derived from chromaticity analysis of Landsat digital data (Figure 3). They demonstrated the clearer water at the centre of a clockwise gyre in central Minas Basin, the general increase in TSM head-ward through the system, and the seaward movement of sediment along the south shore of Minas Basin. They depicted a series of TSM contour maps under different weather conditions for each season and at various stages of the tide. The maps show that highest TSM values occur during the spring. The average TSM

concentration, in the central part of the Basin, in this season is approximately 60 mg/l. Lowest values occur during the summer (1 - 5 mg/l), and intermediate concentrations occur during the winter and autumn (40 mg/l). A recent study, using remote sensing images, showed that surface suspended sediment concentration has a strong seasonal variation (Wu *et al*., 2011).

Estimating water quality from remote sensing has four main advantages: the ability to cover large areas, rapid results, low cost, and convenience for dynamic monitoring (Zhang *et al*., 2010). Although mapping of TSM concentrations can be achieved from space-based optical sensors and has growing applications related to sediment transport, several investigators have demonstrated that standard ocean-colour products from sensors like SeaWiFS and MODIS could not obtain accurate results in high turbidity waters (Shen *et al*., 2010a). Remote sensing of TSM in high turbidity waters (Changjiang estuary and the Bay of Fundy) is quite challenging due to the difficulty of atmospheric correction over turbid water and the empirical nature of the retrieval algorithms, which are limited to a specific range of concentrations, areas and seasons (Shen *et al*., 2010b). Remote sensing data also have other limitations. The principal limitation is that they only provide the surficial TSM concentrations. Another significant limitation is that tidal and atmospheric conditions for the time of the satellite overpasses co-vary with a widely varying combination of the various ground conditions (Amos, 1979).

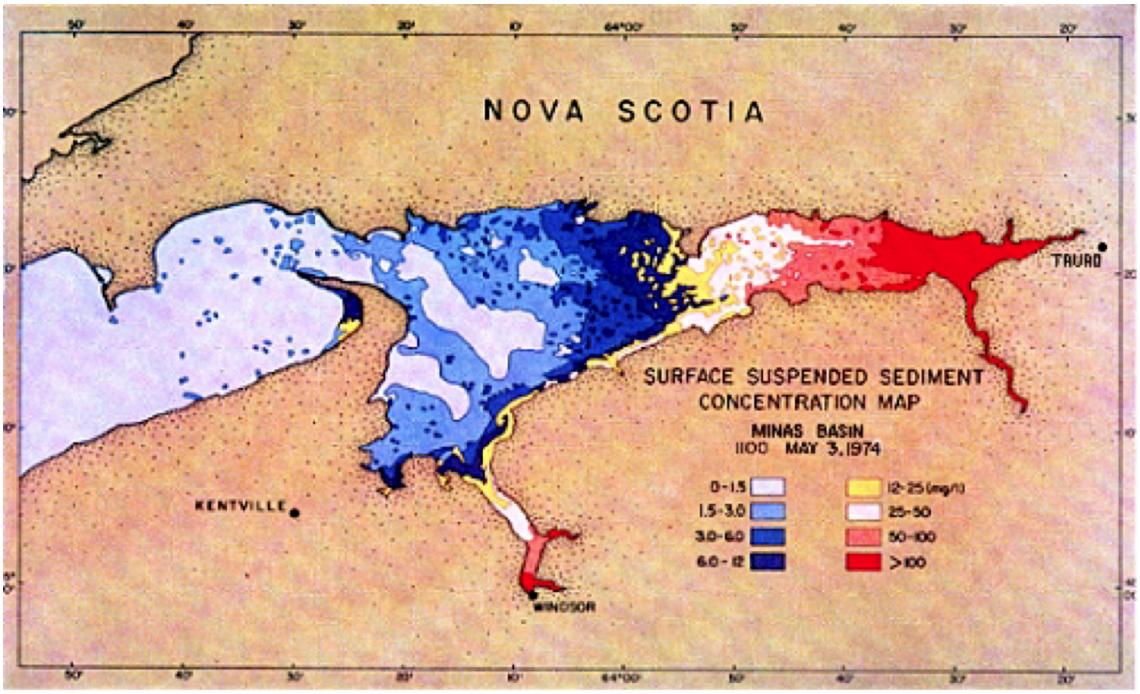

Figure 3: Thematic map of TSM in Minas Basin derived from chromaticity analysis of Landsat digital data 1430 GMT, May 3, 1974, 0.5hr, after high water (Munday *et al*., 1979).

1.3.3 Numerical Modelling

Numerical models can be used to simulate various fundamental physical conditions of the coastal environment such as water level elevations, currents, density stratification and sediment processes. Intertidal areas have frequently been modelled with one-, two- and three-dimensional numerical models. Wood *et al*. (2002) used a simple one-dimensional onshore-offshore model of water movement with a semi-empirical model of cohesive sediment erosion and deposition in Spurn Bright on the north shore of the outer Humber estuary, England. A two-dimensional, depth averaged tidal model was used by Greenberg *et al*. (1983) for studying suspended sediment transport and deposition in Minas Basin. Numerical models like FVCOM (Finite-Volume Coastal Ocean Model) help visualize complex tidal flow changes and sediment transport regimes in the Bay of Fundy. FVCOM is a three-dimensional, finite-volume, unstructured-grid, ocean model developed at the University of Massachusetts-Dartmouth. A high-resolution version of this model has been developed for the Upper Bay of Fundy to simulate the tides and sea level. This model includes the wetting and drying of the extensive tidal flats in Minas Basin,

reproducing the dominant M2 tidal constituent, as well as the total water level in Minas Basin (Dupont *et al*, 2005). Hasegawa *et al.* (2011) and Li *et al*. (2010) discussed the bed load transport in the Bay of Fundy using numerical tidal currents, wave parameters and general circulation features. Wu *et al*. (2011) described the sediment transport in Minas Basin, including bed load and suspended particulate load, and evaluated the model against independent remote sensing images. Generally, the comparison between the model results and observed transport of suspended load shows reasonable agreement. Wu *et al.* also concluded that observed directions of suspension transport are basically reproduced by the model. However, the differences in magnitudes are obvious. The FVCOM model used by Wu *et al.* (2011) clearly overestimates the transport in Minas Basin, but underestimates it in Cobequid Bay, indicating that the results are strongly sensitive to the model input parameters.

The advantages of using numerical models are ability to assess large spatial and temporal scales, ability to focus on effects of specific processes, and ability to make predictions (Greenberg and Amos, 1983). The limitations of numerical models are simplifying assumptions and incomplete understanding of modelled processes, like particle cohesion and suspended sediment density stratification.

1.4 Objectives

In situ measurements, synoptic satellite observations and numerical modelling are mutually beneficial and provide independent sources for inter-comparison and when combined, advance the description and understanding of the spatial-temporal variability of surficial TSM over Minas Basin in the Bay of Fundy. The scientific objectives of this research include:

1. To assemble the observed daily high resolution surficial TSM concentration data in Minas Basin converted from the ocean colour imagery data collected by MERIS satellite over the period of May 2008 - July 2011 in the Bay of Fundy;
2. To conduct the temporal autocorrelation analysis of surficial TSM concentration data with the goal of identifying the dominant time scales of surficial TSM variability in the Bay of Fundy;
3. To examine the results of gridded TSM fields produced by the Delft3D model during different seasons and over the same area;
4. To assess the performance of sediment dynamics models in simulating TSM concentration over Minas Basin, and to identify models strengths and limitations.

1.5 Structure of Thesis

The thesis is organized as follows: Chapter 2 describes data collection from the MERIS satellite, *in situ* measurements, and the Delft3D Model. The methodologies for identifying the dominant time scales of surficial TSM variability and for comparison between maps of TSM are also introduced in Chapter 2. In Chapter 3, comparisons between the magnitude and spatial and temporal pattern of observed and simulated TSM are presented. Chapter 4 discusses the satellite-derived, seasonal TSM concentration variations and explores factors that could produce mismatch between seasonal changes in modelled versus satellite-derived TSM over the shallow areas. A summary of scientific results and recommendations are given in Chapter 5.

CHAPTER 2 MATERIALS AND METHODOLOGY

2.1 Materials

This section provides information of various observations in the MERIS satellite data and *in situ* data to be used in assessment the Delft3D model in simulating the seasonal sediment dynamics in Minas Basin. The setup and model forcing of Delft3D are also described.

2.1.1 MERIS Satellite

Remotely sensed monitoring of TSM started in 1974 using ERTS-A (Earth Resources Technology Satellite) data (Kritikos *et al.*, 1974). Several studies have demonstrated the capabilities of remote sensing to quantify marine bio-geophysical parameters using different sensors: e.g. Sea-viewing Wide Field-of-view Sensor (SeaWiFS), Moderate Resolution Imaging Spectroradiometer (MODIS), and Medium Resolution Imaging Spectrometer (MERIS) (Shen *et al*., 2010a). MERIS has a higher spectral resolution, signal-to-noise ratio and spatial resolution than other sensors (Bourg *et al*., 2009). The European Space Agency (ESA) launched MERIS as one of the ENVISAT satellite payloads in 2002. MERIS uses passive optical imaging instruments to measure radiation reflected and emitted from the Earth's surface. This section briefly describes the MERIS case 2 water (optically-complex water) algorithm. The algorithm derives the inherent optical properties (IOP) of (1) the absorption coefficient of phytoplankton pigment, (2) the absorption coefficient of *gelbstoff* and total suspended matter after bleaching the phytoplankton pigment fraction and (3) the scattering coefficient of total suspended matter (TSM). The IOPs of (1) and (3) are converted into the concentrations of chlorophyll a and TSM dry weight. The algorithm is based on a neural network, which relates the bi-directional water leaving radiance reflectances to these IOPs (Doerffer and Schiller, 2007). The MERIS algorithm advanced theoretical basis documents are available on *http://envisat.esa.int/instruments/meris/atbd/*. The algorithm for MERIS

satellite estimates of TSM concentrations showed a significant limitation in that only low to moderate concentration (1 to 50 g/m^3) could be reliably estimated (Shen *et al*., 2010a).

The MERIS satellite data are available for download from the ESA website, for the period from 2002 to 2012. Communications with the ENVISAT satellite was lost suddenly on 8th April 2012, and ESA declared the end of mission for ENVISAT. MERIS data have deliverable Level 1b and Level 2 products for users after processing via the ground service segments. MERIS level 2 product groups encompass ocean colour products, land and cloud. MERIS spectral bands and applications are listed in Appendix A. In coastal zones, the apparent optical properties of surface seawater are determined according to the concentrations and inherent optical properties of 4 groups of substances: pure sea water, phytoplankton (and associated organic matter), total non-chlorophyllous suspended matter, and coloured dissolved organic matter (yellow substance or *gelbstoff*) (MERIS product handbook, 2002). Total non-chlorophyllous suspended matter is assumed to be solely composed of non-absorbing mineral particles, so a more appropriate name would be 'total suspended mineralic matter' which is characterised by high scattering coefficients. The non-chlorophyllous suspended matter concentration is expressed by its total scattering coefficient at 550 nm [b_p (550); m^{-1})], and it is converted from optical units (backscatter in m^{-1}) to geophysical units (concentration in g/m^3) using a fixed conversion factor derived for measurements on water samples using a GF/F filter (Doerffer and Schiller, 2007; MERIS product handbook, 2002). The TSM in this thesis is denotes total non-chlorophyllous suspended matter, which is assumed to be inorganic sediment.

The MERIS products are available at two spatial resolutions: Full Resolution (FR) with a resolution at sub-satellite point of 300 m and Reduced Resolution (RR) with a resolution at sub-satellite point of 1200 m. In this study, the MERIS FR images were acquired in the inner Bay of Fundy over the period of May 2008 to July 2011. In general, the MERIS satellite overpasses the inner Bay of Fundy area during 1330 to 1530 GMT every day. Carla Caverhill and Cathy Porter, at the Bedford Institute of Oceanography (BIO), provided the FR MERIS image subsets of small areas around Nova Scotia

covering the inner Bay of Fundy. The MERIS imagery from BIO includes all level 2 products described above. Imagery was further processed using software IDL (Interface Description Language). The MERIS standard products applied in this study are "mapped total suspended matter", "mapped latitude", and "mapped longitude". The MERIS imagery provided by BIO covers the area between 44.80° and 46.10°N and between 63.31° and 65.70°W. The MERIS suspended matter product is an estimate of the suspended sediment concentration in Log_{10} (g/m^3). The MERIS image of TSM concentration on February 10th, 2010 is shown (Figure 4). This image was taken in clear atmospheric conditions and is one of the best acquired by MERIS for this region.

In this study, imagery has been cropped using MATLAB software. The cropped images cover only the Minas Basin, with latitude extending from 45.05° to 45.41°N and longitude from 63.42° to 65.56°W. Cropped images were processed using IDL. For each of the TSM images, SeaDAS and IDL software packages were used to determine the spatial average TSM concentration with a small pixel box (3×3 pixels; ~ 1 km^2). MATLAB software was used to replace the value zero to NaN (Not-a-Number) for pixels in each TSM images. Time series of TSM values in that small pixel box were generated through the whole period. A time series of mean TSM concentrations in the centre of Minas Basin is presented in Figure 5.

MERIS TSM products were used in a previous study to assess TSM levels within the Northumberland Strait based on geographical range, seasonality, weather, and tides (Bugden *et al.,* 2007). That study examined the accuracy of the MERIS TSM calibration, by comparing MERIS with *in-situ* observations on October 17th, 2006 (Figure 6). MERIS TSM is a mean value over a 3×3 pixel box area closest the sample sites. Surface samples were collected from fishing vessels. A scatterplot of TSM estimated by MERIS versus *in-situ* TSM shows that points fall along a 1:1 line, indicating that MERIS imaging reliably estimated TSM concentrations in the coastal zones.

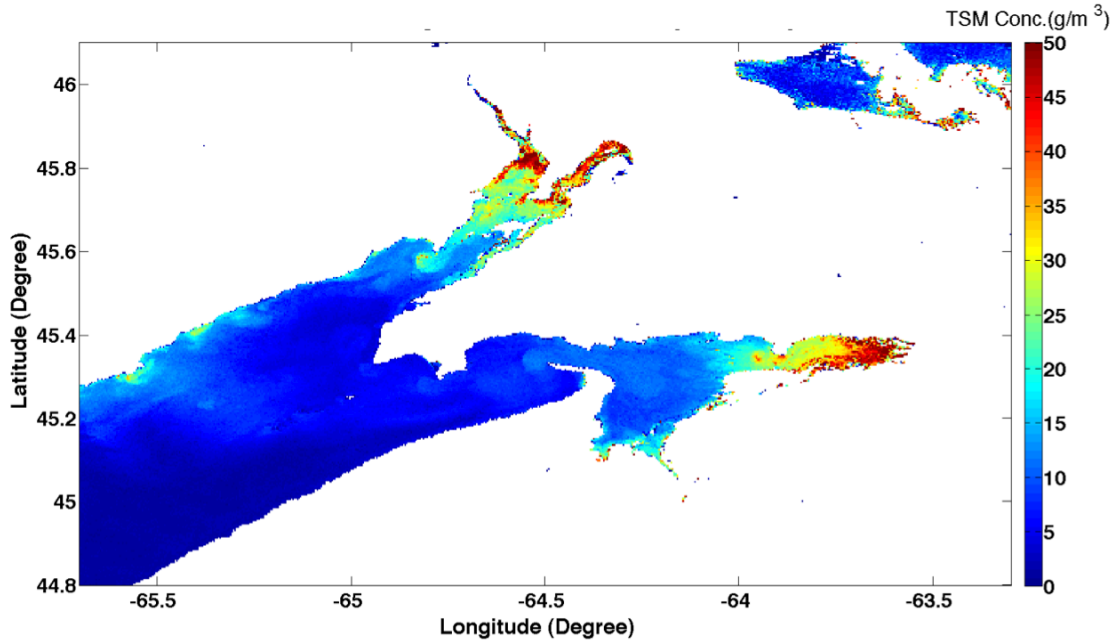

Figure 4: Concentrations of total suspended matter (TSM; g/m^3) derived from a MERIS image in the upper Bay of Fundy on 1506 GMT, February 10th, 2010.

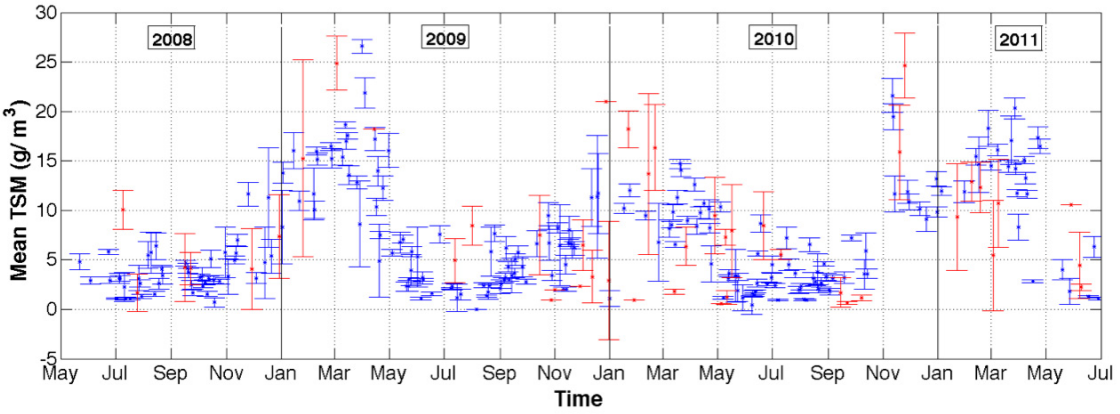

Figure 5: Time series of mean values of TSM over a 3×3 pixel box surrounding the A5 mooring site (A5: 45.239° N, 64.264° W) in Minas Basin from May 2008 to July 2011. Blue dots indicate data from all nine pixels were used in the average (valid); Red indicate fewer than nine pixels were used (invalid). Error bars indicate +/- 1standard deviation of TSM concentration values in the pixel box.

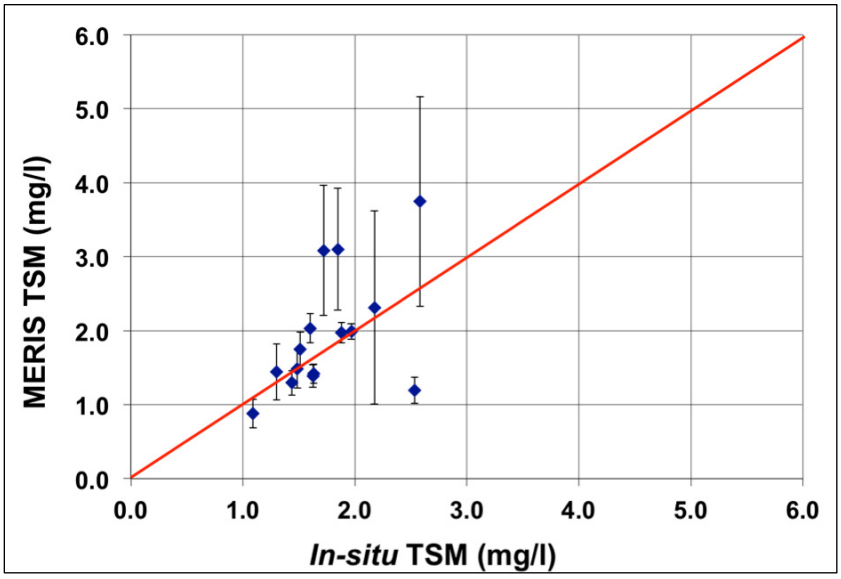

Figure 6: Comparison of TSM concentrations of MERIS and *in-situ* observations within the Northumberland Strait on October 17th, 2006. Error bars indicate +/- 1standard deviation of MERIS TSM (modified from Budgen *et al.*, 2007)

2.1.2 *In situ* Data

The historical *in situ* TSM data in the Bay of Fundy have been assembled in order to assess the satellite-derived TSM. Unfortunately, only limited data exist for the surficial TSM concentration in the Bay of Fundy.

Amos and Joyce (1977) presented the TSM concentrations in Minas Basin, including concentrations as a function of location, depth, and time. There were 11 sites located in Minas Basin and 2 sites located outside of the Basin. Note that data for station 5 in Amos and Joyce (1977) were not available (Figure 7). Table 1 lists the site location, period of observation, depth of water of the stations and tidal characteristics of the stations occupied during the offshore survey of the water quality in Minas Basin. The surficial (0 - 1 m) TSM concentrations data relative to time at stations were pick out. The mean and standard deviation (SD) of surficial TSM during the observation period were calculated and are listed in Table 2.

TSM concentration data also were collected by Brent Law (BIO) from a cruise on March 29th, 2012 at a particular location (A5: 45°14.40'N; 64°15.50'W). The TSM

profiles are listed in Table 3. Cobequid Bay lies at the eastern end of Minas Basin and at the head of Cobequid Bay is the town of Truro, located at the mouth of the Salmon River Estuary (Figure 7). Crewe (2004) provided *in situ* TSM concentrations at the mouth of Salmon River Estuary as a function of depth. The mean concentration at 0 m depth is around 50 g/L during the whole summer in 2000.

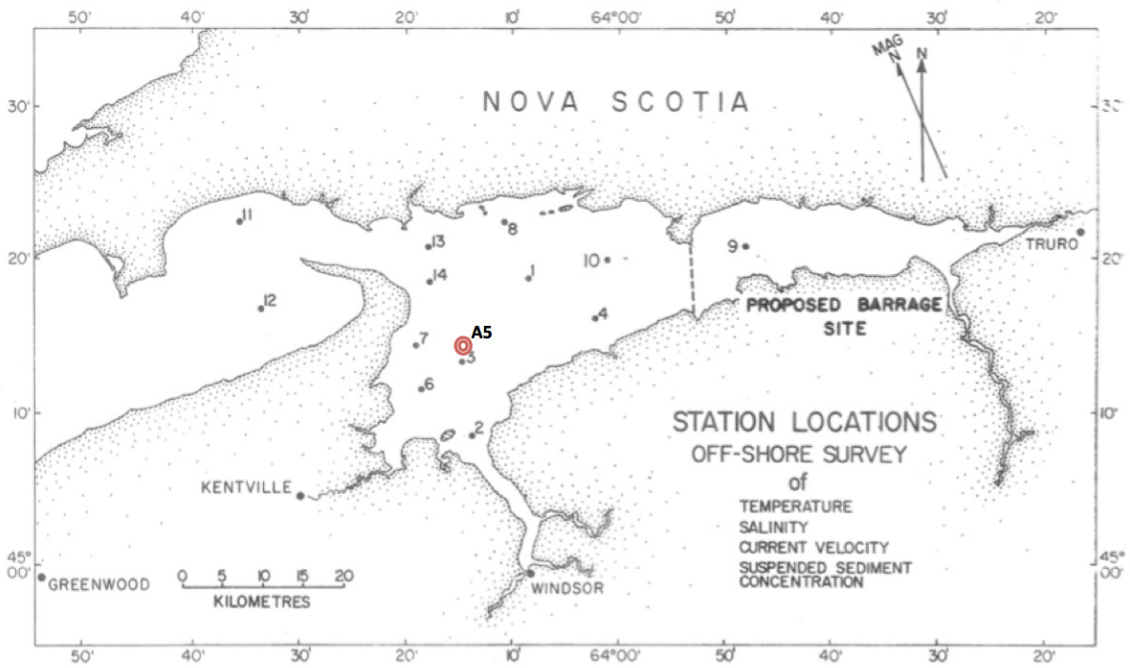

Figure 7: Sites of suspended sediment survey in Minas Basin (modified from Amos and Joyce, 1977). Site A5 (red dot) is located over the central Minas Basin and has been occupied for various times in 2008-2013.

Table 1: The location, period of observation and tidal characteristics of the stations occupied during a survey of the water quality in Minas Basin (Amos and Joyce, 1977).

OFF-SHORE STATION LOCATIONS

Temperature; Salinity; Suspended Sediment Concentration; and Current Velocity

STATION	DATE	LONGITUDE	LATITUDE	WATER DEPTH(M)	RANGE (NORM to 1.0)		TIDAL CYCLES
1	10/7/75	64°18'55"	45°11'40"	16.4	0.83	Wave rider buoy location	2
2	23/7/75	64°13'20"	45°08'25"	5.5	0.74	Avon river bell buoy	1
3	8/8/75	64°15'15"	45°13'20"	11.0	0.89	Cross sands shoal bell buoy	1
4	24/8/75	64°02'15"	45°15'40"	3.6	0.68	Walton bar	1
6	10/8/75	64°18'55"	45°11'40"	3.7	0.94	Cornwallis/Gaspereau estuary	1
7	11/8/75	64°19'20"	45°15'10"	18.3	0.91	Blomidon point	1
8	6/9/75	64°11'00"	45°22'10"	5.5	0.92	The Brother/Pinnacle Isl.	1
9	22/6/76	64°18'10"	45°20'45"	11.0	0.51	Cobequid Bay	1
10	9/6/76	64°01'10"	45°19'50"	7.3	0.60	The brick kiln	1
11	10-11/11/76	64°35'56"	45°22'26"	27.4	0.63	Diligent River (Dawson)	3
12	11-12/11/76	64°34'00"	45°16'36"	29.3	0.51	Scotts Bay (Dawson)	2
13	22-23/6/76	64°18'05"	45°20'45"	62.2	0.55	Parrsboro/Minas Passage (Dawson)	4
14	23-24/5/76	64°18'00"	45°18'40"	51.2	0.54	Cape Blomidon/Minas Passage (Dawson)	2

Table 2: The mean and standard deviation of surficial TSM (0 - 1 m) for various dates in 1975-76 at Amos and Joyce (1977) sites in Minas Basin.

Station	Mean TSM (mg/L)	SD
1	6.440	3.220
2	26.994	13.497
3	7.315	3.658
4	6.143	3.071
6	12.078	6.039
7	4.528	2.264
8	3.506	1.753
9	8.471	4.235
10	11.409	5.705
13	4.785	2.392
14	5.459	2.729

Table 3: The TSM profile collected at Location A5 on March 2012 (Atlantic time).

Time	Surface (0 m)	5 m	10 m	2 m off bottom
	TSM (mg/L)	TSM (mg/L)	TSM (mg/L)	TSM (mg/L)
8:30	27.9	27	34.8	36.1
9:30	25.6	N/A	N/A	20.9
10:30	27	23.1	31.8	32.4
11:30	21.8	31.1	31.4	34.9
12:30	28.4	26.2	31	31
13:30	32	33	31.4	27.5
14:30	31.6	31	26.8	31.4
15:30	25.6	14.7	27.2	27.5
Mean	27.5	26.6	30.6	30.2

2.1.3 Delft3D Model Set-up

The numerical modelling system used in this study is Delft3D, which is a numerical hydrodynamic and morphologic model developed by WL|Delft Hydraulics, now called Deltares. This modeling software was first developed in the 1980s and has evolved during the past decades to be one of the premier models for simulations of flow circulation, sediment transport, waves, water quality and morphological changes over coastal waters (Sutherland *et al*., 2004). This modelling platform can make two- and three-dimensional computations for oceanic, marine, coastal, estuarine and river areas (Borsje, 2006). Delft3D is now open-source and is composed of several modules, such as the FLOW module and sediment transport module. The hydrodynamics, including river and tidal flows, density-driven mixing and shear stress calculations, are simulated in the FLOW module (Lesser *et al.*, 2004). Lesser *et al*. (2004) provided a detailed description of the model underlying equations and showed that the coupled hydrodynamic and sediment modules are capable of simulating many of the important processes that are relevant in coastal environments, including suspended sediment transport.

Delft3D-FLOW is a multi-dimensional (2D or 3D) hydrodynamic model, which calculates non-steady flow resulting from tidal forcing currents and water level elevations, wind stress at the surface and pressure gradients due to the free surface slopes and density gradients on a curvilinear, boundary-fitted grid. These equations are derived from three-dimensional Navier Stokes equations for incompressible free surface flow, under the assumption of shallow water and the Boussinesq approximation (Borsje, 2006). A full description of the formulation and implementation is given in the Delft3D-FLOW manual (WL|Delft Hydraulics, 2006). There are three primary advantages of the DELFT3D-FLOW model: (1) it is simple and efficient to use the standard implicit transport solver in the flow model to compute the transport of suspended sediment; (2) the density effects of suspended sediment concentrations on the flow can be taken into account; (3) views of the distribution of suspended sediment concentrations over large spatial and temporal areas can be generated (Lesser *et al.*, 2004).

This section gives on overview of the model implementation of sediment transport in Delft3D-FLOW. Delft3D-FLOW resolves the water motion based on the bathymetry and boundary conditions, and flow is further determined by the setting of a range of physical parameters. The transport of fine suspended sediment is usually calculated from the local instantaneous flow conditions (Borsje, 2006). The transport of fine suspended sediment in the model is based on the advection-diffusion equation (Equation 1 below). Delft3D schematizes the different sediments as either 'cohesive', 'non-cohesive' or 'bed load'. 'Non-cohesive' transport is a combination of both suspended and bed load transport. As this study focuses on suspended sediments at the sea surface, this section deals primarily with 'cohesive', and only one fine sediment fraction is used.

The three-dimensional suspended sediment transport is calculated by solving the following advection-diffusion equation for each control volume for one sediment fraction (WL|Delft Hydraulics, 2006):

$$\underbrace{\frac{\partial c}{\partial t}+\frac{\partial uc}{\partial x}+\frac{\partial vc}{\partial y}+\frac{\partial (w-w_s)c}{\partial z}}_{advection}+ \underbrace{-\frac{\partial}{\partial x}\left(\varepsilon_{s,x}\frac{\partial c}{\partial x}\right)-\frac{\partial}{\partial y}\left(\varepsilon_{s,y}\frac{\partial c}{\partial y}\right)-\frac{\partial}{\partial z}\left(\varepsilon_{s,z}\frac{\partial c}{\partial z}\right)}_{diffusion}=0 \quad (1)$$

where:

c = mass concentration of sediment [kg m^{-3}]

u, v, w = flow velocity components [m s^{-1}]

$\varepsilon_{s,x}, \varepsilon_{s,y}, \varepsilon_{s,z}$ = eddy diffusivities in three directions [m^2 s^{-1}]

w_s = settling velocity of suspended sediment [m s^{-1}]

In Equation 1, the geographic coordinate system of velocity is defined as positive eastwards, northwards and upwards. The settling velocity w_s is positive downwards, so the sign is negative here. Equation 1 can only be solved if all the time-dependent boundary conditions are specified. These include the conditions at the start of the computation (initial condition), at the horizontal boundaries of the system, at the water surface, and at the bed. The initial condition specifies what the concentration of sediment

is in each grid cell at t = 0. The sea surface boundary condition is that the flux of sediment across the air-sea interface is zero.

$$-w_s c - \varepsilon_{s,z} \frac{\partial c}{\partial z} = 0, \qquad \text{at } z = \zeta \tag{2}$$

where:

ζ = the sea surface elevation [m]

The second boundary condition is prescribed at the bed. The exchange of material through this bottom boundary is modelled by the fluxes between the bottom-most water layer and the bed.

$$-w_s c - \varepsilon_{s,z} \frac{\partial c}{\partial z} = D - E, \qquad \text{at } z = z_b \tag{3}$$

where:

D = deposition flux of suspended matter [kg m^{-2} s^{-1}]

E = re-suspension flux [kg m^{-2} s^{-1}]

z_b = the location of the bed [m]

For the mud sediment fraction, the deposition (D) and erosion (E) terms are calculated with the well-known Partheniades-Krone formulations (Lesser *et al*., 2004):

$$E = M \cdot S\left(\tau_{cw}, \tau_{e\_crit}\right) \tag{4}$$

$$D = w_s \cdot c_b \cdot S\left(\tau_{cw}, \tau_{d\_crit}\right) \tag{5}$$

where:

M = first order erosion rate (erosion parameter) [kg m^{-2} s^{-1}]

τ_{cw} = maximum bed shear stress due to current and waves [N m^{-2}]

$S\left(\tau_{cw}, \tau_{e\_crit}\right)$ = erosion step function defined as

$$S\left(\tau_{cw}, \tau_{e\_crit}\right) = \left(\frac{\tau_{cw}}{\tau_{e\_crit}} - 1\right), \quad \text{when } \tau_{cw} > \tau_{e\_crit},$$

$$= 0 \qquad \text{when } \tau_{cw} \leq \tau_{e\_crit}.$$

c_b = average sediment concentration in the near bottom computational layer [kg m^{-3}]

$S(\tau_{cw}, \tau_{d\_crit})$ = deposition step function defined as

$$S(\tau_{cw}, \tau_{d\_crit}) = \left(1 - \frac{\tau_{cw}}{\tau_{d\_crit}}\right), \quad \text{when } \tau_{cw} < \tau_{d\_crit},$$

$$= 0 \qquad \text{when } \tau_{cw} \geq \tau_{d\_crit}.$$

τ_{e_crit} = critical bed shear stress for erosion [N m^{-2}]

τ_{d_crit} = critical bed shear stress for deposition [N m^{-2}]

In this study, a boundary-fitted grid in spherical coordinates has been developed for Minas Basin covering a domain of approximately 110 km in the east-west direction and 45 km in the north-south direction, with an open boundary across Minas Channel (18 km west of Cape Split), which is an inflow open boundary.

The vertical sediment transport is mainly affected by the sedimentation and re-suspension flux (Figure 8), which are affected by the settling velocity (w_s) and erosion parameter (M) respectively. In the model, the bottom shear stress (τ_{cw}) plays an essential role in defining whether or not sedimentation of suspended particles or erosion of bed material will occur. Sedimentation takes place when the bottom shear stress drops below a critical value (τ_{d_crit}). On the other hand, erosion occurs when the bottom shear stress exceeds the critical value for re-suspension (τ_{e_crit}). The bottom shear stress is based on the shear stress due to currents and waves (Borsje, 2006). The suspended sediment advects and diffuses vertically from lower layer $\sigma = k$ to upper layer $\sigma = k - 1, \ldots \sigma = 2, \sigma = 1$.

Delft3D was used by Dr. Ryan Mulligan of Queen's University to simulate the hydrodynamics and sediment dynamics in Minas Basin. Working with Dr. Mulligan, I helped develop the sediment input parameter sets, processed the model results and compared with the observations.

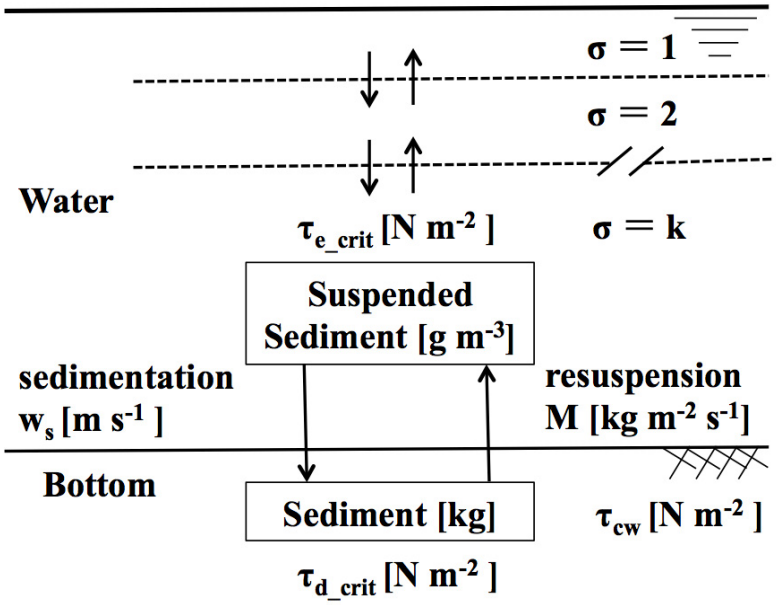

Figure 8: Governing parameters for sedimentation and re-suspension of sediment (modified from Borsje, 2006)

The circulation model for Minas Basin has a horizontal resolution of 200 m, and the vertical resolution is variable with 10-layers in topography-following coordinates. The Delft3D model domain in Minas Basin is shown in Figure 9. The sediment included in the model is cohesive fine sediment only. In model test runs coarse sand was included, but its concentration in the surface layer was insignificant because of it large settling velocity. In later runs sand was not included in the model because the focus of the inter-comparison of modelled and measured TSM concentration is at the sea surface, which is visible to the MERIS satellite.

The parameters required to model cohesive sediment include critical bed shear stresses for erosion τ_{e_crit} and deposition τ_{d_crit}, the erosion parameter M and the particle settling velocity w_s. For the fine suspended sediment, the settling velocity varies in time and space as a result of flocculation (Winterwerp, 2002). The critical stress for bed erosion is a complex variable, dependent on the antecedent stress history of sediment and on the *in situ* bulk sediment properties, whereas the critical deposition stress is a function of grain properties of the suspended material, concentrations and salinity (Amos and Mosher, 1985). The sediment samples collected near Windsor in Minas Basin and Evangeline

Beach, which are both located in Minas Basin, exhibited a high critical erosion stress. Additionally, a theoretical critical shear for the Windsor samples was found to be about 3.3 N/m^2 estimated from the relationship of Smeardon & Beasley (Amos, 1985). This theoretical value of τ_{e_crit} was about 41% of the actual measured value. Amos (1985) used the values of τ_{d_crit} in the range from 0.121 to 0.100 N/m^2 in testing the sediment accumulation rates on Windsor Bay. They found that the use of τ_{d_crit} of Creutzberg & Postma produced the closest approximation to the observations made in the field (Amos and Mosher, 1985). The settling velocity for the surface sample was set to 0.4 mm/s. Amos (1985) also provided a table for the erosion parameter of corrected salt water. The erosion parameter at which the suspended sediment concentration became linear through time was 7×10^{-4} kg/m^2/s. The default value of the erosion parameter in Delft3D-FLOW model is 1×10^{-4} kg/m^2/s.

The values of parameters used for simulations were varied (Table 4). In the model runs, w_s was varied between 0.1 to 0.5 mm/s, τ_{e_crit} was varied between 1 to 2 N/m^2, τ_{d_crit} was set to 0.2 N/m^2, and M was varied between 5×10^{-6} to 5×10^{-5} kg/m^2/s. Only the top-level TSM concentration was used in this work. The vertical resolution is variable with 10-layers in topography-following coordinates in Minas Basin, so the vertical layer thickness at the surface varied between locations.

Bottom sediment is allowed to suspend by erosion from the seabed in the model. As the result, the seabed sediment distribution must be specified. An example of known bottom sediment distributions from observations (reported in Greenberg and Amos, 1983) is shown in Figure 2. Based on this map, it can be noted that various sediment types exist on the seabed, with complicated spatial distributions in Minas Basin. However, most sediments are non-cohesive (sands to gravels) with particles that have relatively high settling velocities. Fine cohesive sediments (muds) occur in several locations around the rim of the basin, namely the Cornwallis River estuary, the Avon River channel, near Economy Point and in Scot's Bay. Based on this, a basic bi-modal distribution map was created for input to the model, graphically shown in Figure 10. This map consists of an initial seabed of mud in water depths of 10 m and less (mean sea

level) and no sediment in depths greater than 10 m.

The other initial conditions for the model are: 1) flow velocity components $u, v, w = 0$ m/s, 2) water surface elevation $\eta = 0$ m and 3) TSM = 0 kg/m^2. The amplitude and phase of the M2 tidal constituent were specified at the model open boundary. The period of this lunar tidal constituent is 12.42 h. This is the dominant tidal constituent over the region and can be considered to be representative of general tidal forcing (Greenberg and Amos, 1983).

The model skill assessed by comparing predictions of the flow velocity and sediment concentration to observations. Hydrodynamic validation was made through a comparison of velocity components (u, v) with the ADCP (Acoustic Doppler Current Profilers) observations at station A5 in the centre of Minas Basin. Validation of the sediment model was performed similarly. Modelled TSM concentration patterns were compared with satellite-derived TSM patterns at the surface layer in Minas Basin.

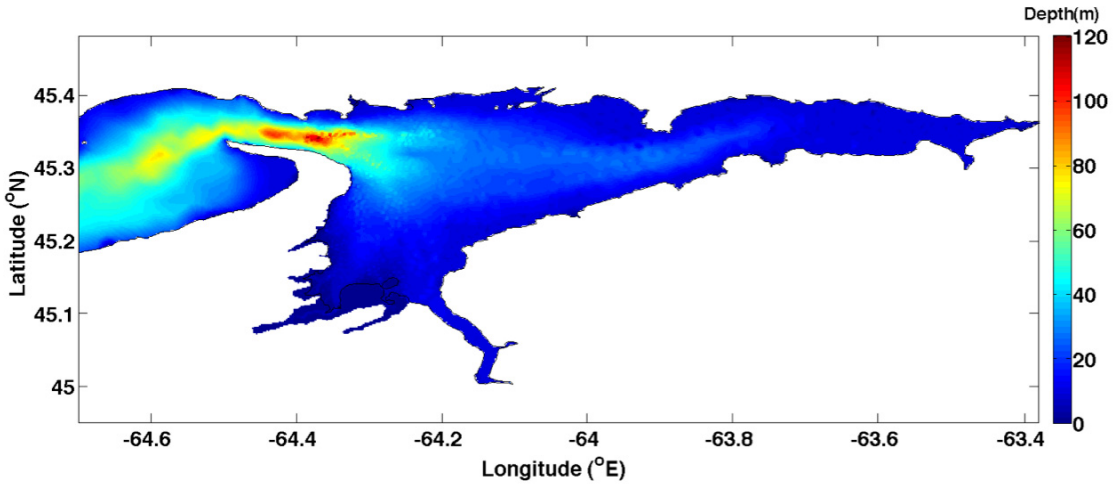

Figure 9: Delft3D-FLOW model domain of Minas Basin in m.

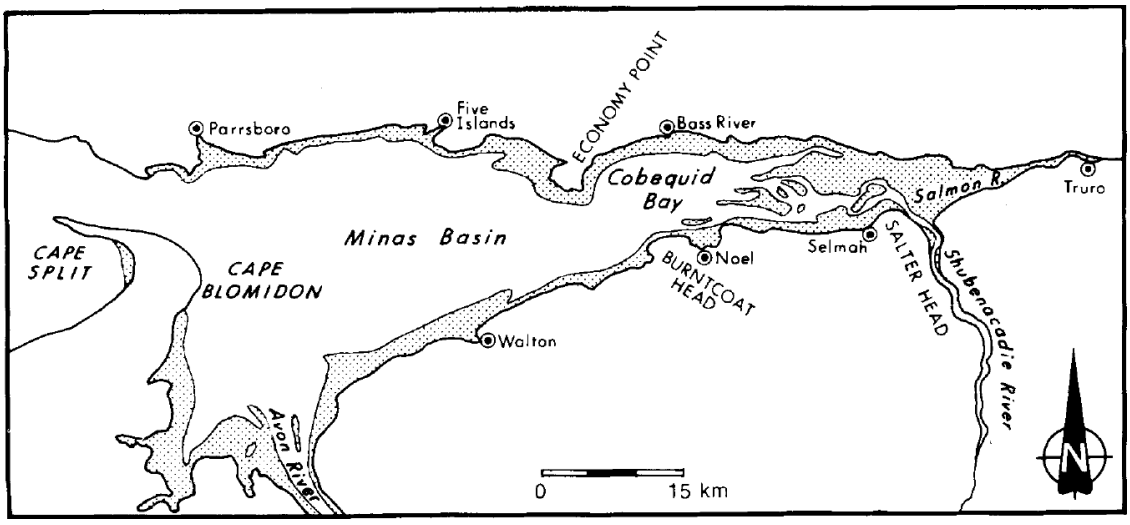

Figure 10: Location map of the intertidal zone in Minas Basin – Cobequid Bay area. Stipple shows the intertidal zone and graphically represents the bottom mud distribution in the model (Dalrymple *et al*., 1990).

Table 4: Summary of Delft3D model sediment input parameters for each run.

Run Number	w_s	τ_{d_crit} **Sediment**	τ_{e_crit} **Erosion**	**Erosion Parameter (*M*)**
	[mm/s]	[N/m^2]	[N/m^2]	[kg/m^2/s]
301	0.1	0.2	2	5×10^{-5}
302	0.1	0.2	2	5×10^{-6}
303	0.1	0.2	1	5×10^{-5}
304	0.1	0.2	1	5×10^{-6}
305	0.5	0.2	2	5×10^{-5}
306	0.5	0.2	2	5×10^{-6}
307	0.5	0.2	1	5×10^{-5}
308	0.5	0.2	1	5×10^{-6}
309	0.1	0.2	2	4×10^{-5}
310	0.5	0.2	1	4×10^{-5}
311	0.4	0.2	1	5×10^{-6}
312	0.5	0.2	1	4.5×10^{-5}

2.2 Methodology

2.2.1 Autocorrelation Analysis

To identify the dominant time scales of variability in the suspended sediment field, statistical analysis was applied to the surficial TSM data. In Minas Basin, time series of satellite-derived TSM concentrations from station A5 reveals seasonal variability and spring-neap variability (Figure 5). It should be noted that the MERIS TSM products are typically unequally spaced in time, which makes spectral analysis difficult. Unequal spacing arises because satellite performance depends on widely varying conditions, such as cloud cover, ground conditions and the water leaving radiance reflectance. Many basic techniques that work well for regular time series are not appropriate for unequally spaced time series, such as satellite TSM data.

A variogram has been used for determining the spatial or temporal correlation of observations. In this study, the variogram was used to estimate the dominant time scales of variability in the suspended sediment field. For a stationary random process $\{Y(t)\}$, the distribution of $Y(t) - Y(t-k)$ does not depend on t. The mathematical definition of the variogram, $V(k)$, is

$$V(k) = \frac{1}{2} E[\{Y(t) - Y(t-k)\}^2] \quad (6)$$

where k is a time lag, and $E(x)$ denotes the expected values of x. For a series $\{y(t_i)$: i=1, … , n$\}$, a plot of the quantities $v_{ij} = \frac{1}{2}\{y(t_i) - y(t_j)\}^2$ against $k_{ij} = t_i - t_j$ for all $^1/_2\, n(n-1)$ distinct pairs of observations is called the empirical semi-variogram (Diggle, 1990). The time lag k is plotted along the horizontal axis and the value of the semi-variogram along the vertical. The k starts at zero, since the lag k is always positive. The v_{ij} axis also starts at zero, since it is an average of squared values.

Since observations are highly irregular in time, there will be more than one v_{ij} corresponding to a particular value of k_{ij}. The sample variogram is simplified by replacing all v_{ij} by their mean value, V(k), leading to a desirable reduction in the amount

scatter in the sample variogram (Diggle, 1990). Then, $V(k)$ is normalized by the variance of the time series, σ^2, producing the normalized sample variogram:

$$V_v(k) = V(k)/\sigma^2 \quad (7)$$

The normalization by the variance is useful because $V(k)$ can be small because large values of Y are similar or because the absolute values of Y are small. The normalization emphasizes lags for which correlation is good. When the $V_v(k)$ value is close to the zero, the time series is highly auto-correlated at a time lag k. Because high autocorrelation is indicative of periodicity, calculation of the variogram can be used to identify the dominant time scales of variability in TSM.

The temporal variogram analysis was applied to the TSM time series at each pixel box of in the entire Minas Basin. The analysis was used to assess how the degree of autocorrelation varies as a function of geographic location in the Basin. The benefit of this approach is that it creates clear maps of where seasonal effects are strongest, providing a simple way to carry out a model-data comparison in the Basin.

2.2.2 Relative Difference

Evaluation of the Delft3D model used in this study involves comparison of model-generated and data-derived spatial maps of TSM concentration. The challenge for skill assessment is determining at what point does one say the two maps are similar or different, and how does one quantify how similar the two maps are in an objective manner (Stow *et al*., 2009).

Comparison using the relative difference (RD) directly capitalizes on the spatial coincidence between grid-based data maps. It simply compares the corresponding values at each grid position. The RD are calculated with the following equation (Berry, 1999):

$$RD = \left[\frac{[map1_{value} - map2_{value}]}{map2_{value}}\right] * 100 \quad (8)$$

This method has several advantages. It is straightforward to calculate, it is easy to interpret, it uses the entire data range, and it depicts relative differences geographically.

In this study, the $map1_{value}$ stands for the simulated model TSM concentration, and $map2_{value}$ stands for the observed satellite TSM concentration. When the RD is larger than 0%, the modelled TSM is larger than the satellite estimation; otherwise the modelled TSM is lower than the satellite estimation. The values of RD were checked to confirm that the absolute values were bounded.

CHAPTER 3 RESULTS

3.1 Satellite TSM Concentration

3.1.1 Time Series and Sample Variogram of Satellite TSM Concentration

The four sites in Minas Basin were selected for the analyses. These four sites are named MB (Minas Basin), WB (Windsor Bay), BH (Burntcoat Head) and CB (Cobequid Bay) (Figure 11).

Time series of satellite-derived TSM concentration show a clear annual cycle at MB in the centre of Minas Basin (Figure 12a). The peak values of TSM concentration were around 40 to 50 g/m^3 in mid-winter (March and April), and different for each year. The peak values of TSM concentration were higher in 2009 and 2011 than in 2010. The lower values of TSM concentration were around 0 to 10 g/m^3 in mid-summer (July and August) (Table 5). The TSM concentrations were variable at this location over the winter. However, the TSM concentrations were relatively stable during the summer, generally remaining between 0 to 10 g/m^3.

The sample variogram of the TSM time series at MB in the central part of Minas Basin highlights the yearly cycle (Figure 12b). Smaller sample variogram values indicate stronger autocorrelation. The sample variogram shows that concentrations are least correlated at time lags of approximately 6, 18 and 30 months (~ 180, 540 and 900 days), and the most strongly correlated at time lags of approximately 12, 24 and 36 months (~ 360, 720 and 1080 days). Values of $V_v(k)$ have more variance when time lag k is over 900 days because, given the length of the time series, there are few observations with lags between them that are this large.

The TSM concentration at WB also varies annually, but concentrations are lower than in the centre of Minas Basin (Figure 13a). The maximum TSM concentration is approximately 20 g/m^3 in late winter at position WB, and the concentration is between 0 to 5 g/m^3 in mid-summer (Table 5). The variogram of the TSM time series at WB is

similar to the variogram at MB, revealing strong correlation at lags of 12, 24 and 36 months (Figure 13b).

The TSM concentration at BH varies annually, but the values have more variance than site MB. The TSM concentrations are much higher than in the centre of the Minas Basin (Figure 14a). The maximum TSM concentration is approximately 85 g/m^3 in late winter at position BH, and the minimum concentration is between 5 to 15 g/m^3 in mid-summer (Table 5). There are no obvious differences between the TSM concentrations in winter and summer. The variogram of the TSM concentration time series at BH shows much weaker correlation at annual time scales (Figure 14b).

The TSM concentrations at CB do not vary annually, and they changed considerably during the entire period. The TSM values ranged from 0 to 90 g/m^3 (Figure 15a) (Table 5). The sample variogram of the TSM time series at CB shows no correlation at annual time scales (Figure 15b).

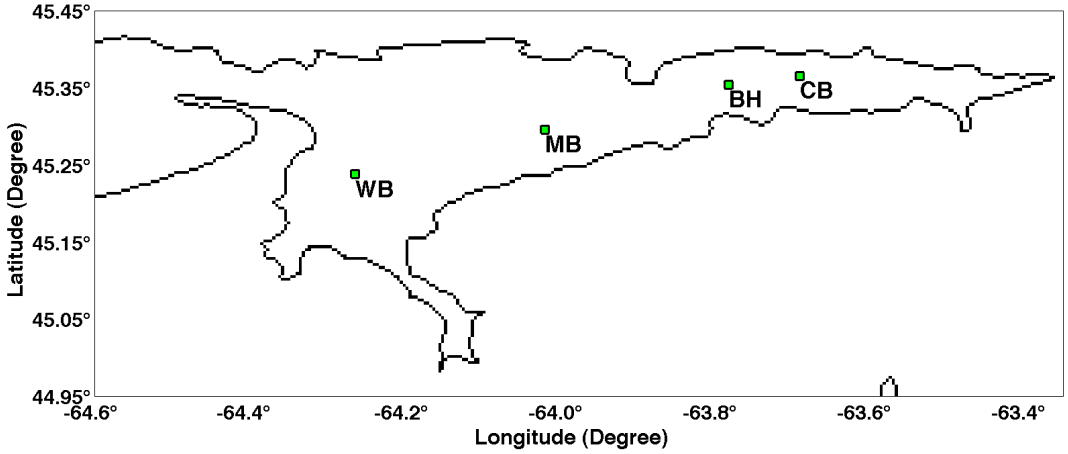

Figure 11: Positions of four sites in Minas Basin, at which TSM concentration time series are used in analyses.

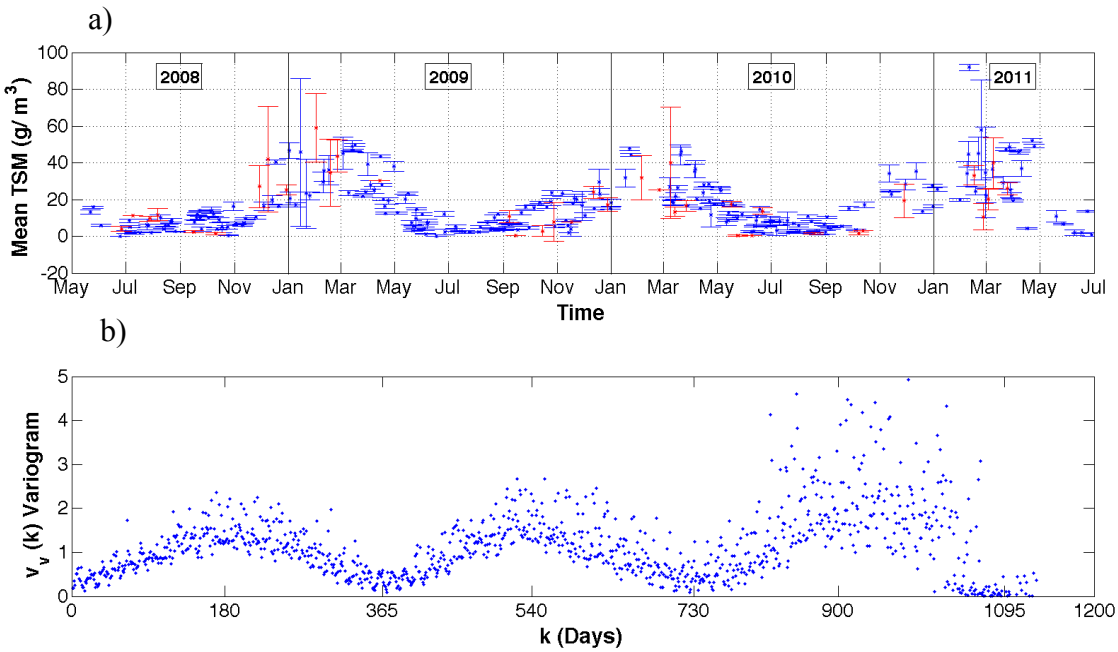

Figure 12: Time series of TSM concentration derived from the MERIS satellite: a) mean values of TSM concentration over a 1 km^2 pixel box (3×3 pixels) at MB in the centre of Minas Basin from May 2008 to July 2011; b) sample variograms of TSM at same location. In the top panel, the blue dots present TSM data for which all nine pixels were used in the average, and red indicate fewer than nine pixels were used. Error bars denote the standard deviation of TSM concentration values in the pixel box. In the bottom panel, smaller values indicate stronger autocorrelation. The normalized variogram shows that concentrations are least correlated at time lag of approximately 180 days.

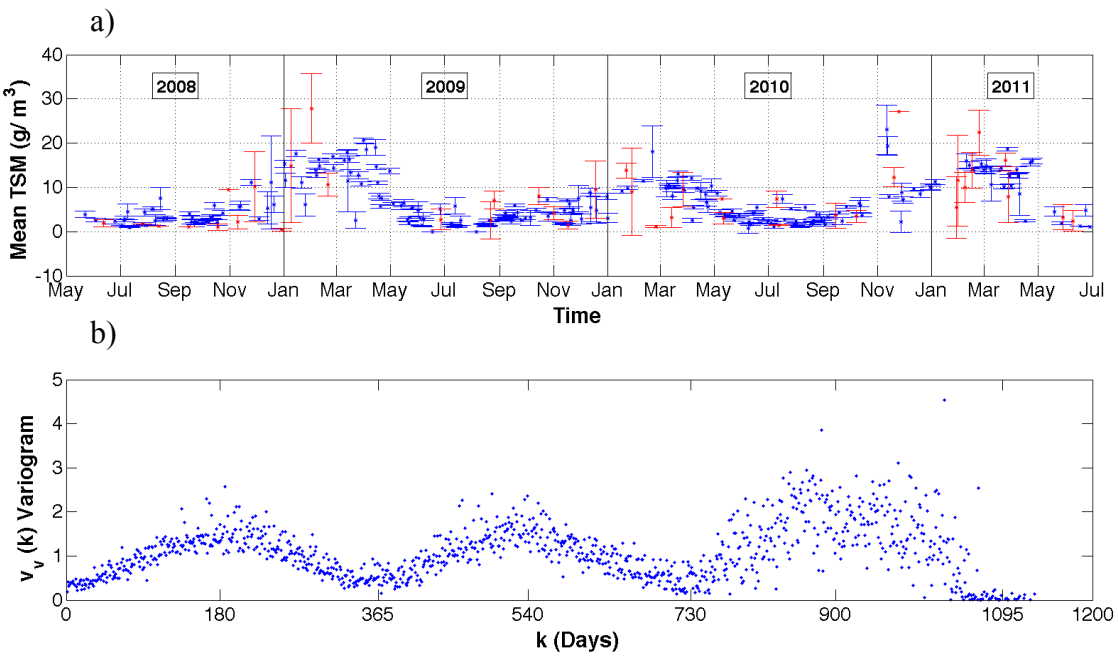

Figure 13: Time series of a) TSM concentration derived from the MERIS satellite and b) variogram calculated from the time series at site WB.

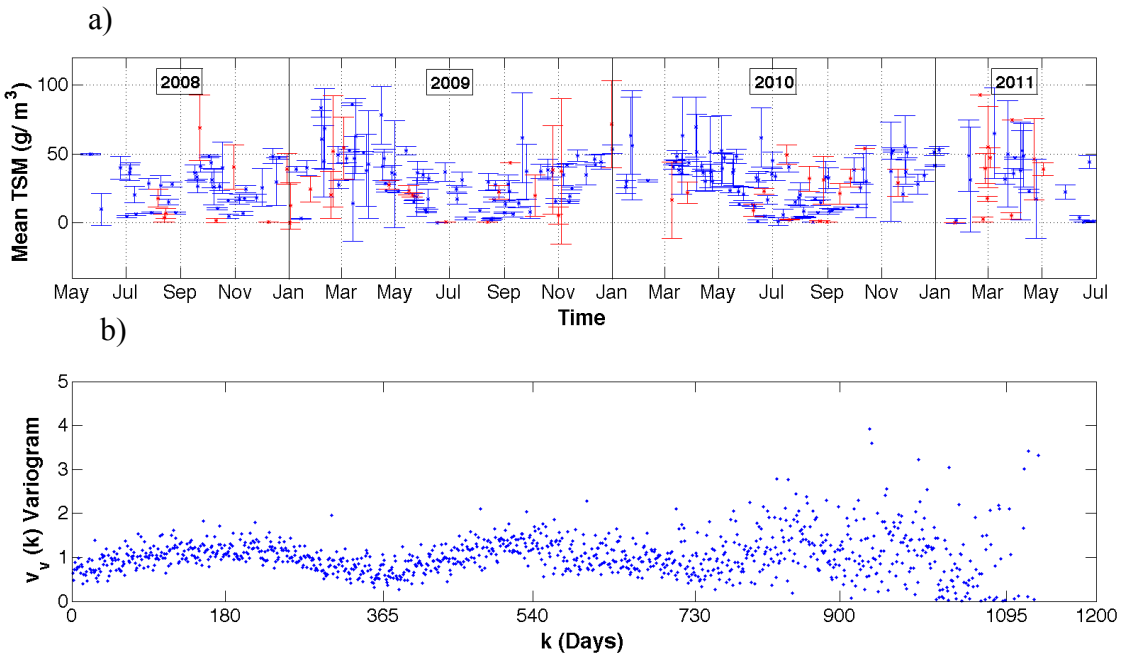

Figure 14: Time series of a) TSM concentration derived from the MERIS satellite and b) variogram calculated from the time series at site BH.

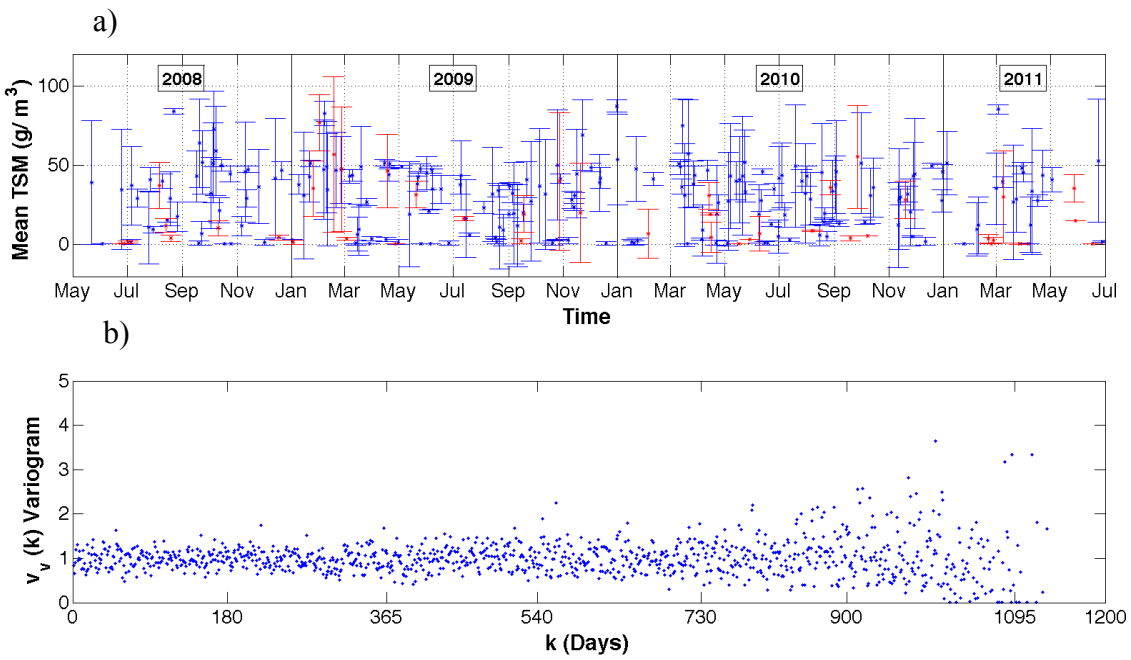

Figure 15: Time series of a) TSM concentration derived from the MERIS satellite and b) variogram calculated from the time series at site CB.

Table 5: Summary of site locations and TSM concentration in Minas Basin.

Site Name (initial)	Latitude	Longitude	Max. (g/m^3)	Min. (g/m^3)	Figure No.
Minas Basin (MB)	45.2962°	-64.0186°	40 ~ 50	0 ~ 10	12
Windsor Bay (WB)	45.2731°	-64.2637°	20	0 ~ 5	13
Burntcoat Head (BH)	45.3538°	-63.7811°	85	5 ~ 15	14
Cobequid Bay (CB)	45.3654°	-63.6892°	(0 ~ 90)		15

3.1.2 Seasonal Variability of Satellite TSM Concentration

An alternative method for examining the annual variability in TSM concentration is to examine maps of the mean TSM in each pixel box in late summer and winter (Figure 16). The summer period is defined here to include just two months, July and August. The winter period contains February and March. In 2009 there are 26 satellite images in summer and 38 images in winter. Most of the mean TSM values were between 0 to 10 g/m^3 in the central Minas Basin and between 10 to 20 g/m^3 in Cobequid Bay and Windsor Bay in summer. In winter, the TSM concentrations increased eastward and southward, and the TSM values were between 15 to 35 g/m^3 in the central Minas Basin, and between 30 to 50 g/m^3 in Cobequid Bay and Windsor Bay.

Similarly, another method for examining annual variability in TSM is to examine the maximum TSM concentration in each pixel in late summer and winter 2009 (Figure 17). The maximum TSM concentration is defined here as the middle value of the largest three concentration values. This definition limits the effect of outliers on estimates of maximum TSM concentration. In summer, the maximum TSM values were between 5 to 15 g/m^3 in the centre of Minas Basin and between 20 to 50 g/m^3 at Cobequid Bay and Windsor Bay (Figure 17a). The maximum TSM values varied from 20 to 40 g/m^3 in the central Minas Basin and higher than 30 g/m^3 at shallow areas (Cobequid Bay and Windsor Bay) in winter 2009 (Figure 17b). The spatial distribution patterns are similar for both the mean and maximum TSM concentrations in Minas Basin.

The seasonal changes in satellite TSM concentrations were estimated by dividing the differences between summer and winter TSM concentrations by the winter TSM concentrations for each pixel box over the entire area (Equation 8). Using TSM in winter as $map2_{value}$, satellite mean TSM concentrations showed seasonal variability in Minas Basin in 2009 (Figure 18). Because the TSM concentrations in winter were higher than in summer, the RD were negative. The summer-winter differences were largest in the northern Basin, given the largest negative RD at -90%.

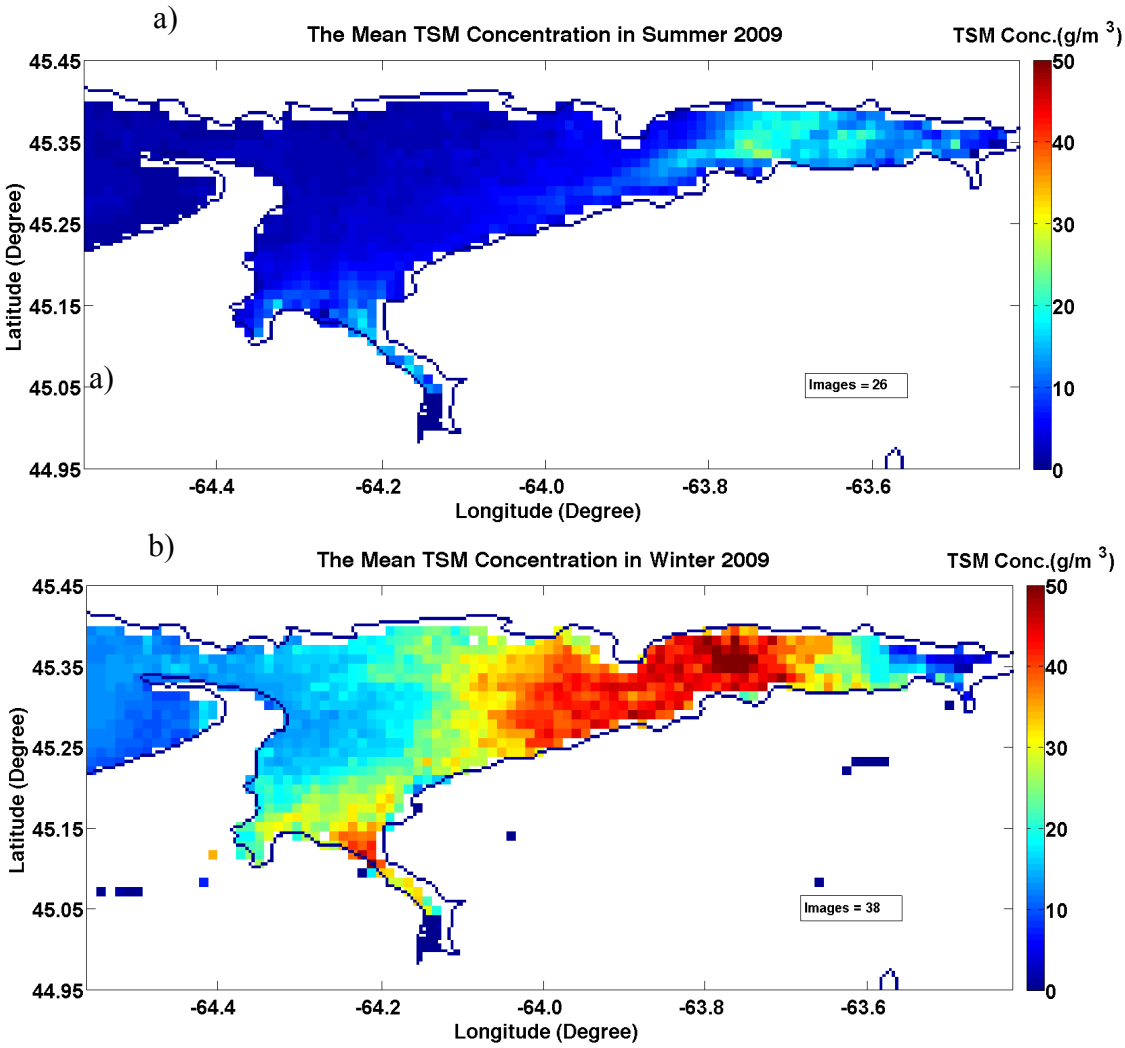

Figure 16: Distributions of time-averaged satellite-derived mean TSM concentration estimated from MERIS images during a) Summer and b) Winter 2009 in Minas Basin. Largest concentrations, shown in warm colours, occurred in Cobequid Bay and in Windsor Bay. Smallest concentrations occurred in Minas Passage. Over the basin, the mean TSM concentrations were higher in winter than in summer.

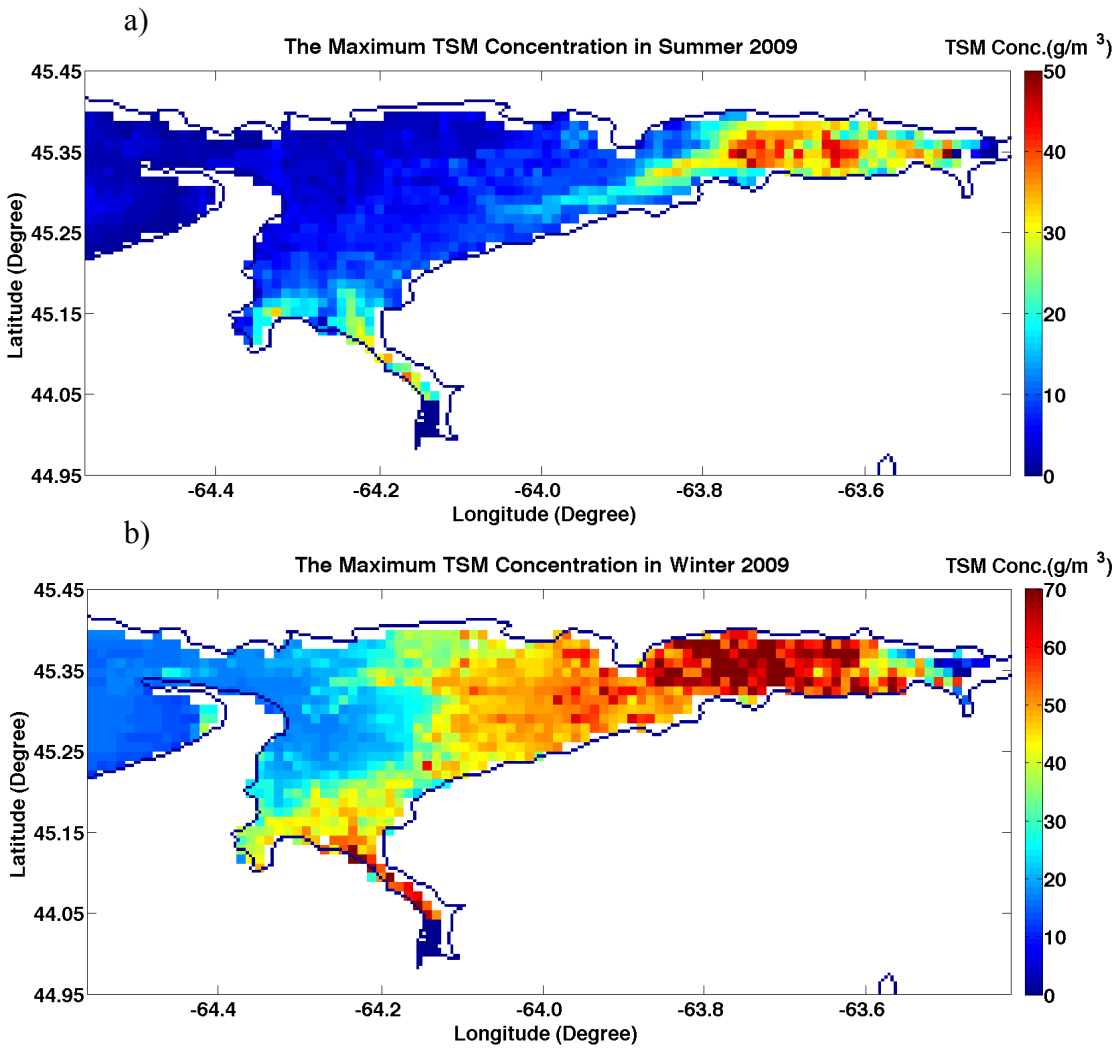

Figure 17: Distributions of maximum satellite-derived TSM concentration estimated from MERIS images during a) Summer and b) Winter 2009 in Minas Basin. Different colorbar scales are use in the two panels. Largest concentrations, shown in warm colours, occurred in Cobequid Bay and in Windsor Bay. Smallest concentrations occurred in Minas Passage. Over the Basin, the maximum TSM concentrations were higher in winter than in summer.

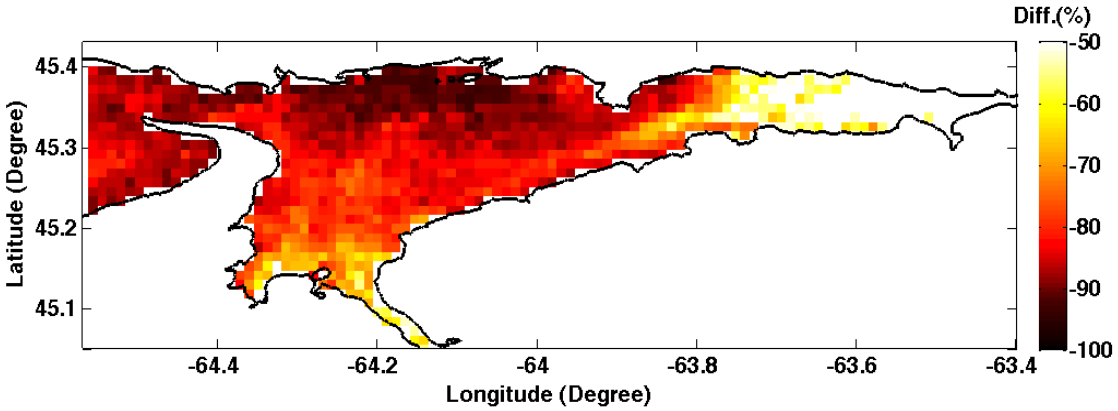

Figure 18: Satellite TSM concentration seasonal differences between summer and winter, normalized by winter values, in 2009 in Minas Basin.

3.2 Strength of Annual Signal

The spatial pattern of normalized sample variograms $V_v(k)$ at 1-year lag is examined to understand the geographic distribution of the strength of the annual signal of satellite TSM concentration. As indicated earlier, smaller sample variogram values indicate stronger autocorrelation. The minimum value of sample variograms between time lag k is ± 30 days of 365 days (1 year) was plotted (Figure 19). Over the central Minas Basin, the $V_v(k)$ ranges between 0.05 and 0.15 indicating that the satellite TSM displays a stronger annual signal. The annual signal is weak in Cobequid Bay, southern Windsor Bay and around coastlines. The black dots around the shorelines are noise. The white (no signal areas) generally have high but variable TSM throughout the year. The warm color areas shown in Figure 19 have the higher TSM seasonal variability.

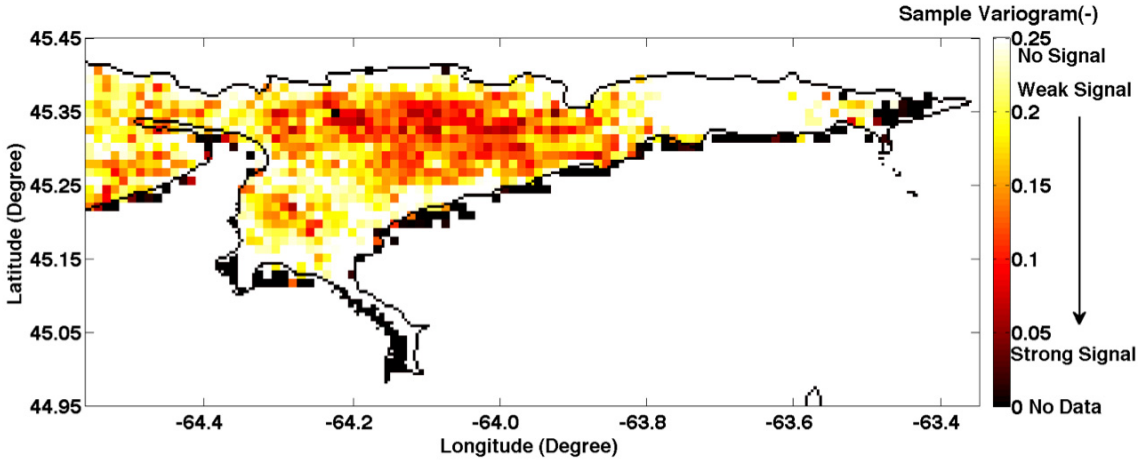

Figure 19: Distributions of estimated annual change in TSM concentration observed by the MERIS satellite, where normalized sample variogram is the minimum value during k = ± 30 days of a year. Lower values indicate larger annual variation and are represented by darker colours.

3.3 Delft3D Model

3.3.1 Delft3D Hydrodynamics

The Delft3D-FLOW model was integrated for 6 to 7 days. Flow velocity and sediment concentration were simulated and compared with observations. Velocities produced by the Delft3D hydrodynamic model compare well with *in situ* observations (Figure 20). As

an example, the velocity observations used in comparisons were collected at 11 m depth at station A5 with an ADCP installed in streamlined floats, with the transducer heads at approximately 4.5 m above the bottom and profile bins set at 4 m resolution. The durations of the data records range from 21 to 41 days. All the records showed good data return with few gaps in the profile over the water column (Wu *et al.,* 2011). The observed currents (speed and velocity components) and model predictions were plotted at ADCP site A5 over a period of four days in July 2009 (Figure 20). Model results at this site and other sites agree qualitatively with the observed tidal amplitudes and phases.

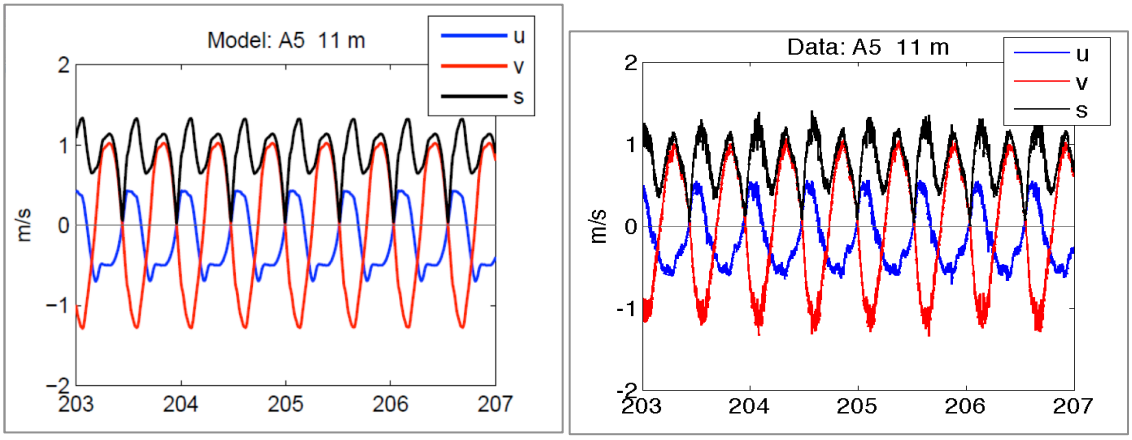

Figure 20: Comparison of observed horizontal current velocity components (u, v) and speed (s) time series at the 11 m depth at site A5 in the Southern Bight of Minas Basin. The x-axis indicates the Julian date in 2009 (July 22-26).

3.3.2 Delft3D Sediment Dynamics

The Delft3D-FLOW model results in the last 2 days of each model run were used to calculate the time-mean fields of TSM. The values of critical bed shear stress for erosion, τ_{e_crit}, and deposition, τ_{d_crit}, the erosion parameter, M, and particle settling velocity, w_s, were varied among simulations (Table 4). The maps of mean concentration of mud throughout in Minas Basin of 300 series are shown in Appendix B (Figures B1-B12).

Run 303 introduced the maximum amount of sediment into suspension (Table 6). Settling velocity and critical erosion shear stress were low, and the erosion parameter was high. Modelled TSM concentrations in the Basin were large as a result (Figure 21a).

Throughout much of Basin, suspended sediment concentrations were over 50 g/m^3. Concentrations this large were observed by the satellite in only in a few areas. Run 306 introduced the minimum amount of sediment into suspension. Settling velocity and critical erosion shear stress were high, and the erosion parameter was low. Modelled TSM concentrations in the Basin were small as a result (Figure 21b). Throughout all of Basin, suspended sediment concentrations were below 10 g/m^3. Concentrations observed by the satellite were higher than this in the shallow areas. Run 303 and Run 306 demonstrated the parameter ranges in the model that produced TSM that encompassed the observed values.

Runs 310 and 311 were the best able to reproduce winter and summer TSM concentration, respectively. For Run 310, settling velocity had a high value, critical erosion shear stress had a low value, and the erosion parameter had an intermediate value. Modelled TSM concentrations in the Basin are similar to those observed in winter (Figure 22a). Suspended sediment concentrations were approximately 50 g/m^3 in Cobequid Bay and Windsor Bay. Suspended sediment concentrations ranged from 15 – 30 g/m^3 in the central part of Minas Basin. For Run 311, settling velocity had an intermediate value, critical erosion shear stress had a low value, as did the erosion parameter. Modelled TSM concentrations in the Basin were similar to those observed in summer (Figure 22b). Throughout the entire Basin, suspended sediment concentrations were below 20 g/m^3. TSM concentrations in shallow areas were higher than in the central Basin.

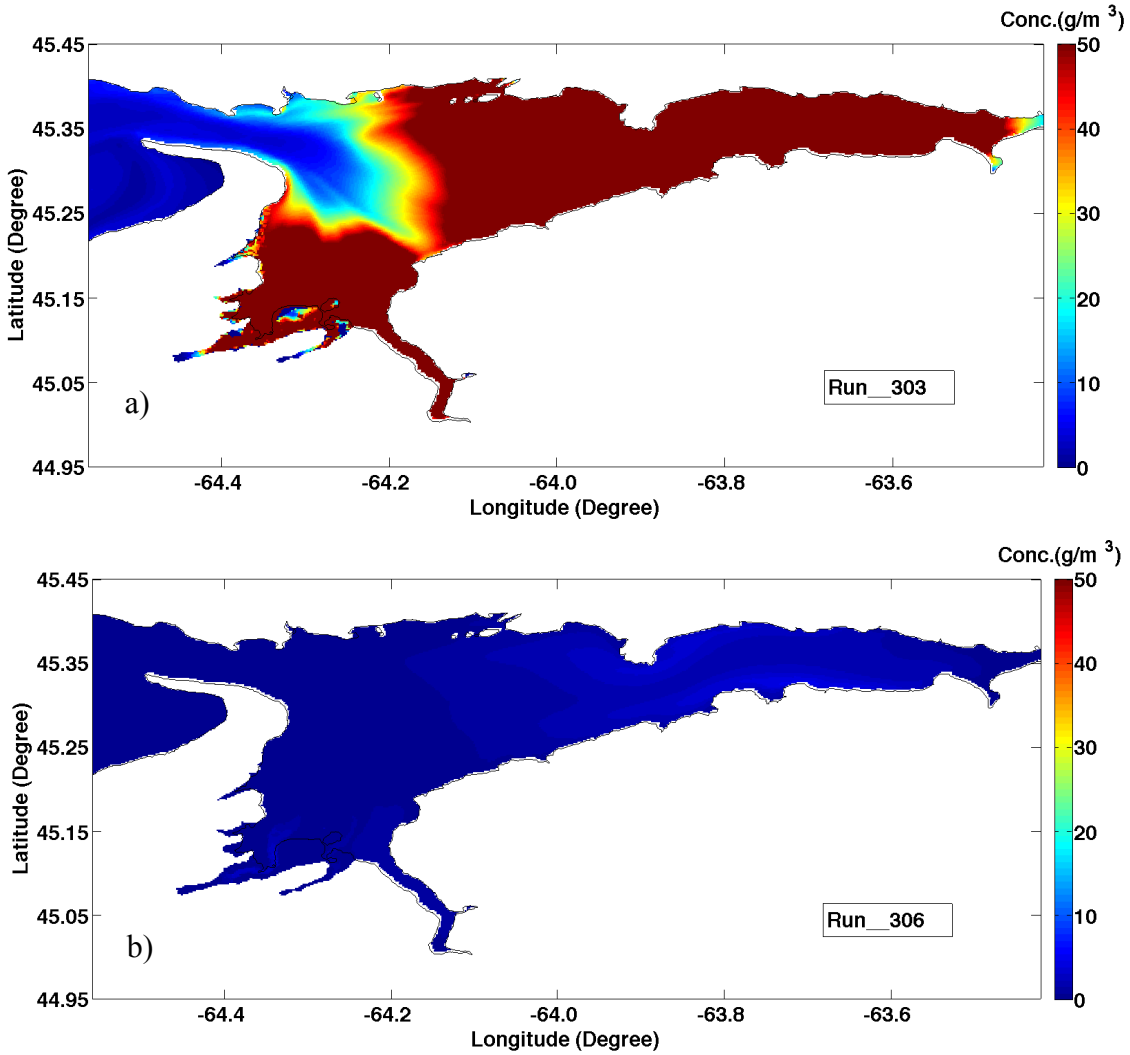

Figure 21: Runs showing the a) maximum and b) minimum amount of TSM concentration simulated by Delft3D with given parameters (listed in Table 4).

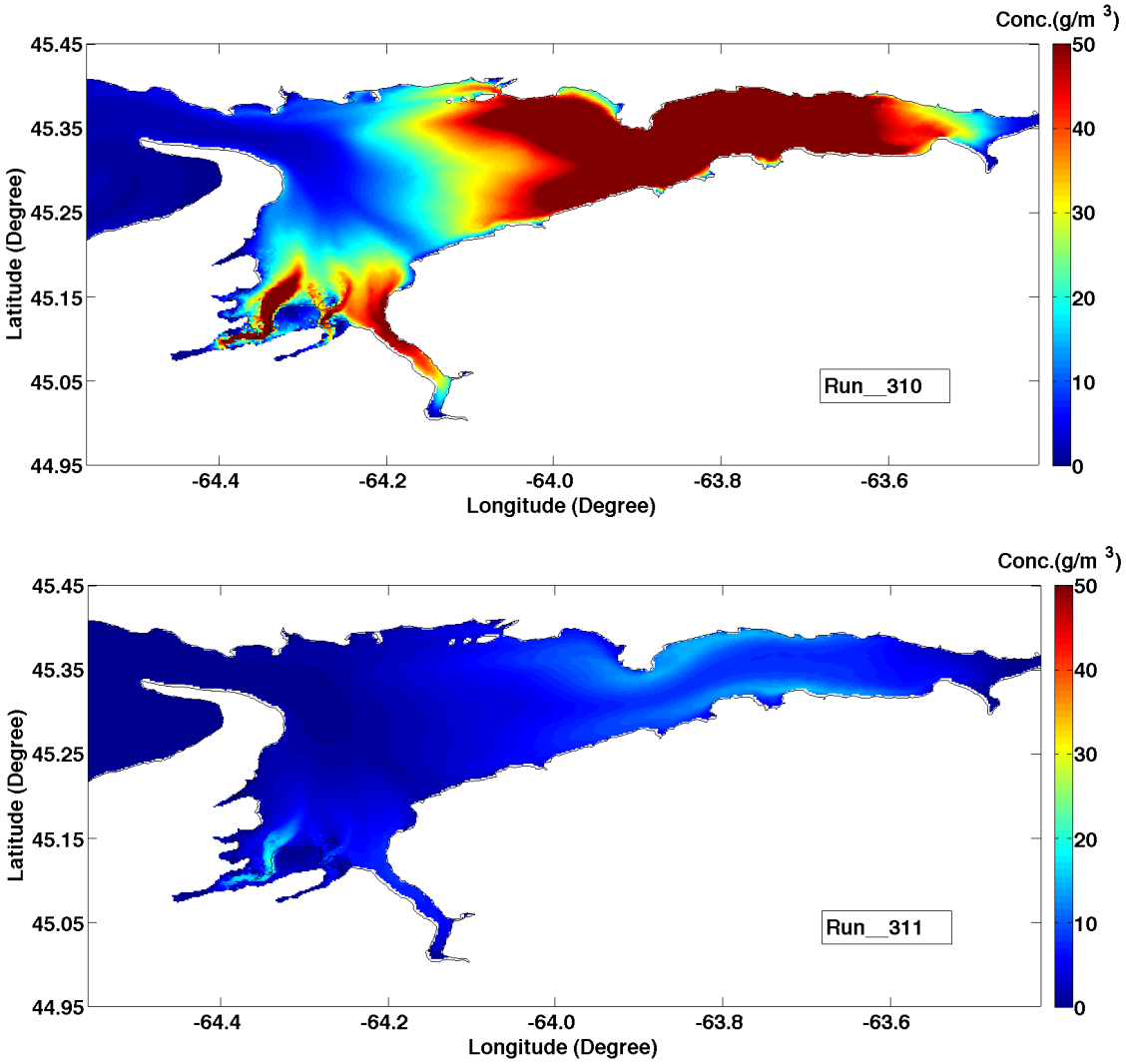

Figure 22: The time-mean concentration of sediment mud simulated by Delft3D model with optimal parameters in Minas Basin.

3.4 Satellite versus Model TSM Concentration

The summer of 2010 and winter of 2009 were chosen for a quantitative comparison between the model results and observations because these two seasons have the largest numbers of satellite images, increasing confidence in the satellite estimates of TSM concentration. The green color in the maps indicates that the RD values are between ± 50%, which is defined in this work as an acceptable difference (Figures 23 and 24). The fraction of pixel boxes that have RD of in the range of ± 50% is termed the "green ratio" (Table 6). Specifically, if the total number of valid pixel boxes for a given map is N, with relative differences of RD_i, i= 1, N, as defined by Equation 8, and the total number of boxes with "acceptable" relative differences, M, defined by $-50\% < RD_i < 50\%$, i=1, M, then the green ratio for that map is M/N. Larger green ratios indicate better agreement between model and satellite TSM concentrations. The largest green ratio for winter 2009 is Run_310 and for summer 2010 is Run_311, which are respectively equal to 49.76% and 49.47%. Sediment distributions for these runs appear in Figure 22.

Model runs 304, 308 and 311 have the largest green ratios in summer (Figure 23, Table 6). These runs share the common feature of using a smaller value for the erosion rate. The spatial variation is different for each simulation for the same season. Run_304 shows better skill at predicting TSM concentration in Cobequid Bay than Run_308 and Run_311, but it overestimates TSM concentration in most areas of the central Minas Basin and southern Windsor Bay. Larger settling velocities in runs 308 (0.5 mm/s) and 311 (0.4 mm/s) leave less sediment in suspension in the deeper Minas Basin, producing better agreement in this area. They also, however, cause under-prediction of concentration over the shallower Cobequid Bay. These runs over-predict TSM at Five Islands and they under-predict TSM in the Minas Passage.

Model runs 301, 310 and 312 have the highest green ratios for winter, again just under 50% (Figure 24, Table 6). These runs share the common feature of using a larger value for the erosion rate. The spatial variation is different for each simulation for the same season. Run_301 shows worse skill at predicting TSM in Cobequid Bay than Run_310

and Run_312, and it overestimates TSM concentration in the eastern end of Cobequid Bay. Smaller erosion parameters in runs 310 (4×10^{-5} kg/m^2/s) and 312 (4.5×10^{-5} kg/m^2/s) leave less sediment in suspension in the deeper Minas Basin, producing better agreement in this area. They also, however, cause over-prediction of concentration over the shallow Cobequid Bay, over a smaller area of Windsor Bay and at Five Islands. Additionally, they under-predict TSM in the Minas Passage.

In summary, model parameters that produced a good agreement between modelled and satellite-derived TSM concentration in the central Minas Basin also produced TSM that were different from satellite-derived estimates in shallow areas. In Cobequid and Windsor Bays, modelled TSM concentrations were higher than satellite-derived estimates in winter. For all model simulations, the modelled TSM concentrations were lower than satellite-derived TSM at Minas Passage. This simplified modelling approach, by varying the sediment parameters in each runs, suggests that the sediment parameters vary in space and time, so a perfect match between model and data will be difficult to achieve in all parts of the Basin.

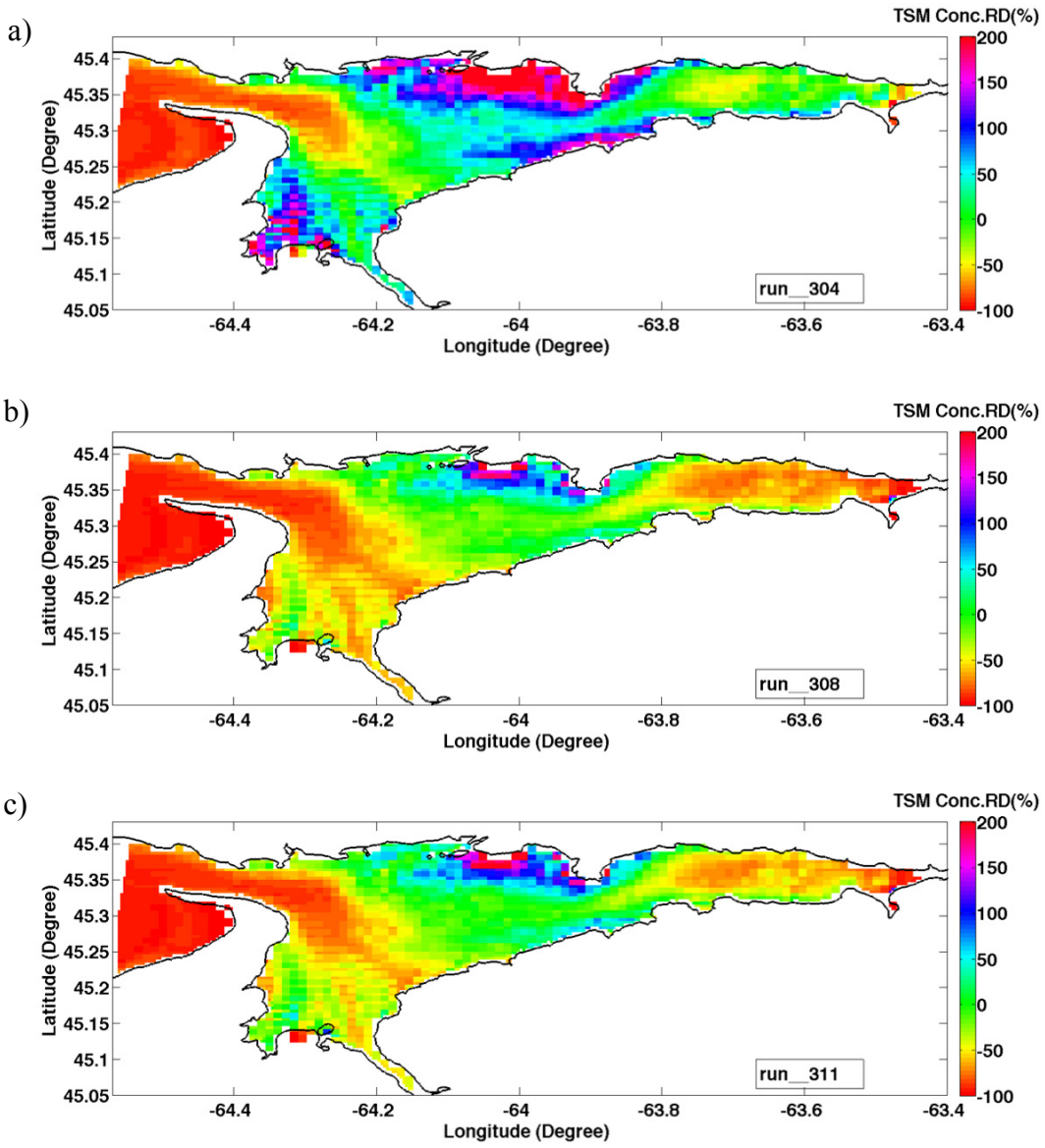

Figure 23: Quantitative comparison between model and satellite-derived TSM concentration during summer 2010 with a) w_s = 0.1 mm/s; b) w_s = 0.5 mm/s; c) w_s = 0.4 mm/s. In a), modelled TSM concentrations were larger than satellite-derived TSM in the northern Minas Basin, in Windsor Bay and near Burntcoat Head. Modelled TSM concentrations were smaller than satellite-derived TSM in Minas Passage. In b) and c), modelled TSM concentrations were closer to satellite-derived TSM in the northern Minas Basin and in Windsor Bay. Modelled TSM concentrations in Cobequid Bay and Minas Passage were less than satellite-derived TSM.

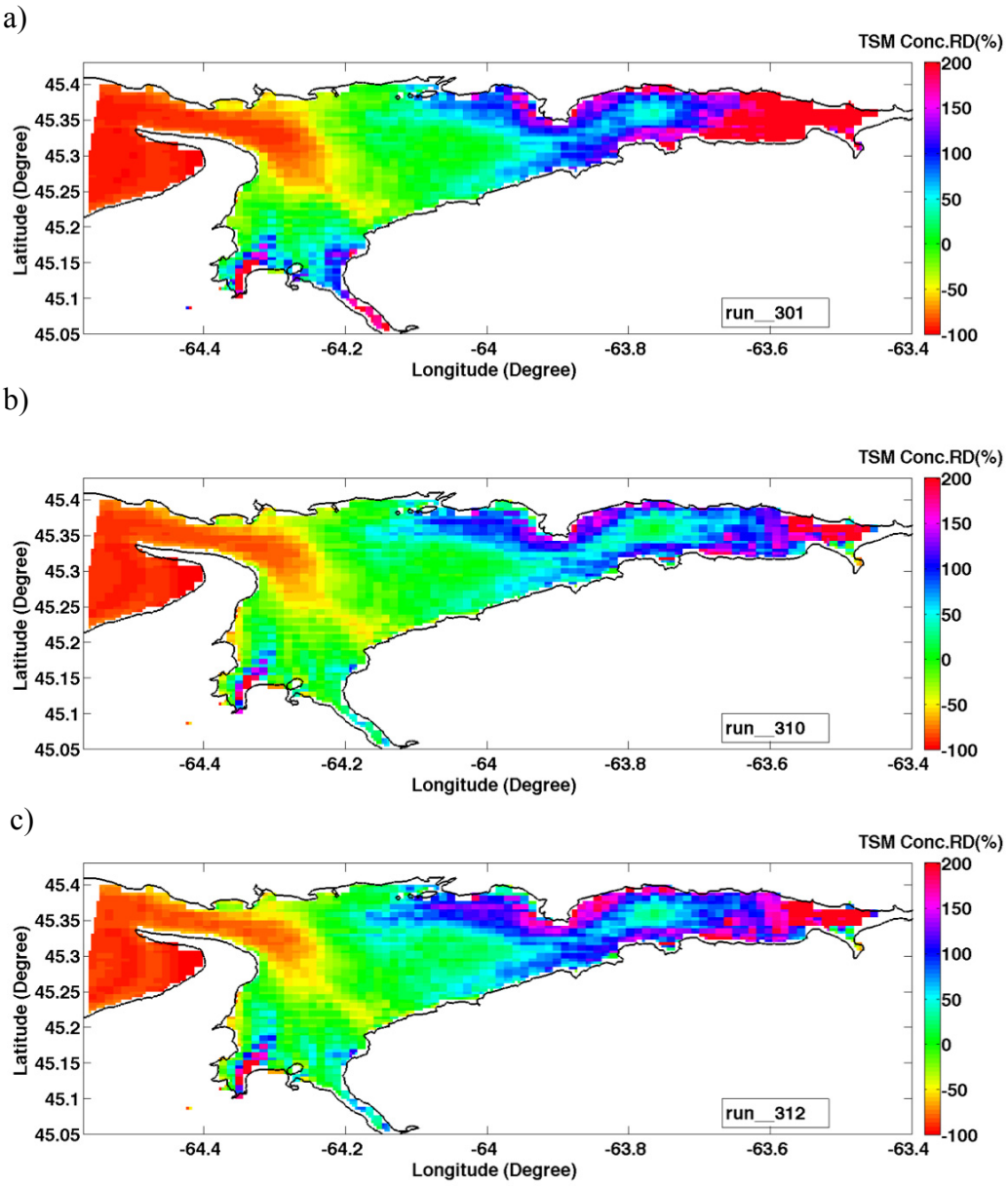

Figure 24: Quantitative comparison between model and satellite-derived TSM concentration during winter 2009 with a) $M = 5\times10^{-5}$ kg/m^2/s; b) $M = 4\times10^{-5}$ kg/m^2/s; c) $M = 4.5\times10^{-5}$ kg/m^2/s. In general, modelled TSM concentrations are similar to satellite-derived TSM through the central Minas Basin. Modelled TSM concentration exceed satellite-derived TSM in Cobequid Bay, and modelled TSM are less than satellite TSM in Minas Passage.

Table 6: List of Delft3D model processing parameters and corresponding green ratio for each run.

Run Number	w_s	τ_{d_crit} Sediment	τ_{e_crit} Erosion	Erosion Parameter	Green Ratio: (|RD|<50%)/total	
	[mm/s]	[N/m^2]	[N/m^2]	[kg/m^2/s]	2009 Winter	2010 Summer
301	0.1	0.2	2	5×10^{-5}	41.68%	-
302	0.1	0.2	2	5×10^{-6}	-	15.16%
303	0.1	0.2	1	5×10^{-5}	11.41%	-
304	0.1	0.2	1	5×10^{-6}	-	44.91%
305	0.5	0.2	2	5×10^{-5}	25.70%	35.62%
306	0.5	0.2	2	5×10^{-6}	-	2.06%
307	0.5	0.2	1	5×10^{-5}	39.72%	-
308	0.5	0.2	1	5×10^{-6}	-	44.52%
309	0.1	0.2	2	4×10^{-5}	36.48%	-
310	0.5	0.2	1	4×10^{-5}	49.76%	-
311	0.4	0.2	1	5×10^{-6}	-	49.47%
312	0.5	0.2	1	4.5×10^{-5}	44.93%	-

Run_310 and Run_311 reproduce seasonal patterns most similar to the winter and summer patterns in TSM resolved by the satellite. These two runs were used to produce the seasonal variability of Delft3D TSM concentration in Minas Basin (Figure 25), based on Equation 8. The difference percentages were approximately -85% over the central Minas Basin and smaller in the Windsor Basin. The RDs between winter and summer modeled TSM vary within a narrower range than winter versus summer differences in satellite TSM (Figure 18 and 25). The two model runs reproduce the factor of 2 difference between TSM in Minas Basin between winter and summer, but they fail to reproduce the minimal change in TSM between winter and summer over the shallower areas of Cobequid and Windsor Bays estimated from the satellite images. This finding indicates either that the satellite is unable to resolve seasonal TSM changes over shallow areas or that the model does not predict TSM accurately over shallow areas.

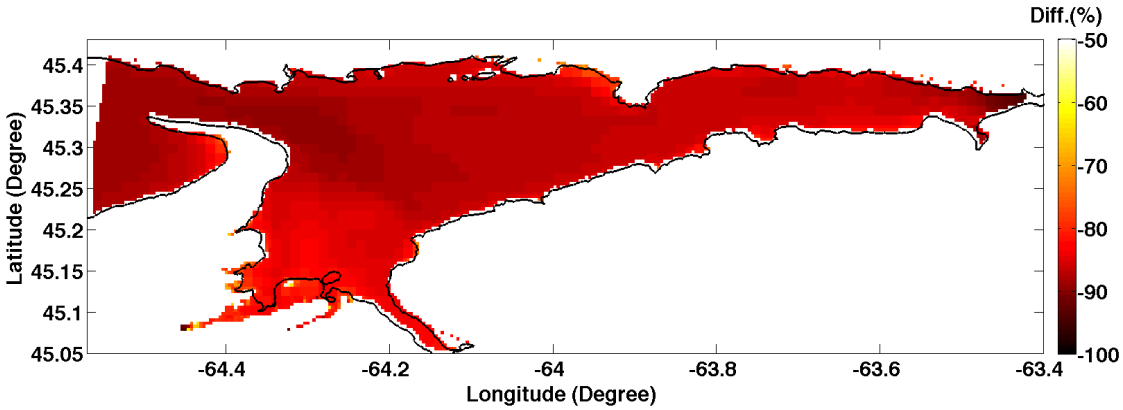

Figure 25: Seasonal variability of Delft3D model TSM concentration in Minas Basin (Runs 310 and 311).

CHAPTER 4 DISCUSSION

Two primary results emerged from the analysis and comparison of modelled and satellite-derived TSM concentration in Minas Basin. First, satellite-derived TSM concentration varied annually, with lower TSM in late summer and higher TSM in late winter. The annual signal was strongest in the central Minas Basin and weaker in the shallow areas of Cobequid and Windsor Bays. The model reproduced the annual variation in TSM concentration by increasing the erosion rate by an order of magnitude for winter simulations. Second, seasonal changes in modelled and satellite-derived TSM concentration did not match over the shallow areas, indicating either that satellite-derived TSM were not accurate in these areas or that modelled TSM were not accurate in these areas. These two results are discussed in more detail in the following sections.

4.1 Strong Annual Signal

4.1.1 Comparison of satellite-derived and *in situ* TSM Concentration

To investigate the accuracy of the satellite-derived TSM concentration in Minas Basin, the observations of satellite-derived TSM concentrations were compared with *in situ* observations. The summer 2010 observations of satellite-derived TSM concentrations and *in situ* TSM concentrations were compared at several locations of the Basin (Figure 26). The SD bars of *in situ* and satellite-derived TSM concentration, which are of width ± 1 SD, overlap, which indicates that the magnitudes of TSM estimated by the satellite are similar to TSM measured *in situ*. A scatterplot of TSM estimated by satellite versus *in situ* TSM shows that points fall close to a 1:1 line (Figure 27). Note that the satellite-derived TSM and the measured *in situ* TSM were collected at the same season (summer). Generally, the satellite-derived TSM concentrations have similar magnitude as *in situ* observations in Minas Basin observation points. However, the *in situ* TSM concentrations are generally higher than satellite-derived TSM. These results may indicate that satellite-derived TSM are underestimates in summer.

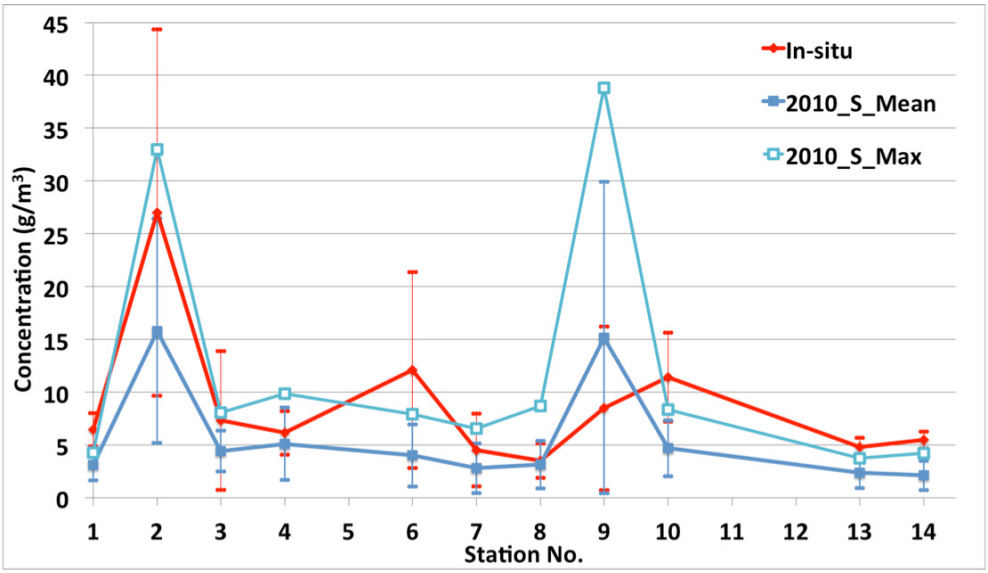

Figure 26: Comparison between *in situ* TSM, satellite-derived TSM and Max. satellite-derived TSM at several sites in Minas Basin. Satellite-derived TSM are from summer 2010, and *in situ* data are from summer 1976 (Amos and Joyce, 1977; Table 1) Red dots denote *in situ* TSM at stations, and error bars indicate ± 1 standard deviation (SD) of TSM. Filled blue dots represent the mean satellite-derived TSM at the same locations. Open blue dots are the maximum concentration of satellite TSM.

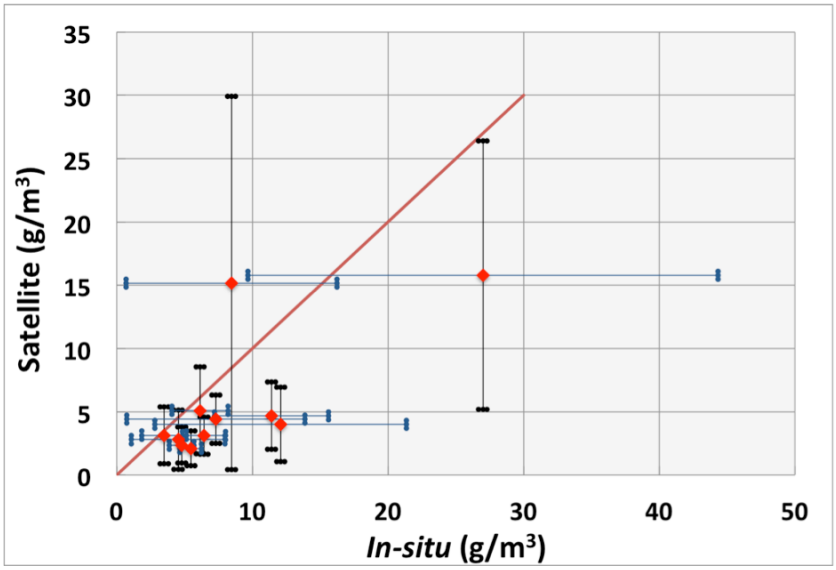

Figure 27: TSM concentration comparison between satellite-derived (2010) and *in situ* (1975-76) measurements at Amos and Joyce (1977) sites in Minas Basin during summer. Error bars indicate ± 1 SD.

In situ TSM concentration at A5 in March 2012 exceeds MERIS TSM estimates from three years, but they are of similar magnitude (Table 7). The two-month (March and April) time-averaged MERIS TSM data were 15.41 g/m^3, 9.12 g/m^3 and 13.09 g/m^3 in 2009, 2010 and 2011 respectively. A time series of hourly *in situ* surficial TSM concentration collected on March 2012 was listed in Table 3, and the 8-hour mean concentration was 27.5 g/m^3. The satellite-derived mean concentrations are approximately a factor of 2 smaller than the mean *in situ* TSM. This result suggests if the underestimation is systematic, then the seasonal cycle will not be significantly affected. Note, however, that *in situ* TSM were collected in the central part of the Minas Basin. Therefore, the annual cycle of satellite-derived TSM in these regions is likely accurate, but the lack an annual signal in shallower regions may or may not be an accurate result.

Table 7: TSM comparisons between MERIS satellite and *in situ* surface measurements at A5 in March and April.

	Date	**Mean (g/m^3)**	**SD**	**Max. (g/m^3)**
MERIS (March and April)	2009	15.41	5.69	26.57
	2010	9.12	3.15	14.70
	2011	13.09	4.56	20.30
In situ	Mar-2012	27.50	3.34	32.00

4.1.2 Causes for Annual Cycle of TSM Concentration

The factors responsible for the annual cycle of TSM variability are unclear, but several possible mechanisms exist. Some plausible reasons for modelled TSM concentration seasonal variability in Minas Basin are discussed below. Annual cycles in TSM concentration may be caused by higher erosion rates in the winter, lower in the summer. Destruction of sediment biofilms may reduce sediment adhesion and induce the higher erosion rates in the winter. Borsje (2006) showed that the small-scale biological activity on the bottom of the seabed has significant influence on the dynamics of cohesive sediment on a large spatial and temporal scale. They used the process-based sediment transport module of Delft3D to assess effects of biology on the Western Wadden Sea. The modelling results indicated that the seasonal variation in the sediment concentration

is caused by wind and biological activity. The Western Wadden Sea is a tidal basin similar to Minas Basin, so it's reasonable to consider that biological activity also has significant influence on erosion rate in Minas Basin. Wave erosion of Triassic sandstone cliffs that surround the shoreline supplies an abundance of sand into Minas Basin (Tomas, 1976; Stea, 2003). Amos (1984) estimated that a total of 3.1×10^6 m^3 of sand is introduced to the system annually from erosion of the cliffs. The cliffs erode at rates of up to 1 m per annum, supplying 1×10^6 m^3 per annum of finer-grained sediment, while a further source of fine-grained material is derived largely from seabed erosion (Amos and Long, 1980). Erosion rates are larger during storms, which are stronger in the winter. Amos and Long (1980) and Greenberg and Amos (1983) argued that sediment concentration at any site within the Minas Basin is controlled by such process as biological activity and wave stirring on the intertidal zone, rather than any other phenomena. Enhanced flocculation in the summer also could account for the decrease in suspended sediment concentration in that season. Flocculation increases the settling velocity of the fine-grained particles by several orders of magnitude (Hill et al., 2000; Mikkelsen et al., 2004), which would lower TSM concentration in the water column in summer.

The annual cycle of TSM concentration in Minas Basin was simulated by altering the erosion rate in Delft3D. This approach attributes the changes in TSM concentration to the effect of biofilms on sediment cohesion. The possibility that increased wave stress results in higher TSM concentration in winter has not been addressed with the model and neither have ice scour processes in winter.

4.2 Accuracy of Satellite-Derived vs. Modelled TSM in Shallow Regions

The results show that, relative to the satellite-derived TSM concentration, the model underestimates TSM at Cobequid Bay and Windsor Bay in summer and overestimates TSM at shallow areas in winter (Appendix C: Figures C1 - C13). It is not clear whether the model or the observations are more accurate in the shallow areas.

4.2.1 Accuracy of Satellite MERIS TSM Concentration

The MERIS sensor may not resolve TSM concentration changes in shallow areas. The problems associated with remote sensing of TSM in coastal waters include difficult atmospheric corrections, confounding effects of phytoplankton, and light scatter from the seabed. The error of the concentration of a water constituent, such as TSM, derived from remote sensing data depends on several conditions. One important condition is that the accuracy of the input data, i.e. the water leaving radiance reflectance, which depends on errors in atmospheric correction. Atmospheric correction for optically shallow waters requires ancillary measurements at the time of image acquisition, which are not possible on a routine basis. The unsolved problem of atmospheric corrections is the limiting factor for remote sensing of coastal waters (C. Mobley, personal communication). The water leaving radiance of shallow coastal waters may also be affected by the reflection of the seabed. Reflectance by sea bottom can be neglected when water depth is much more than signal depth. There is no bottom effect on water leaving radiance when processing MERIS TSM product (MERIS product handbook, 2002).

The Minas Basin area is an extremely complex optical environment. The turbid coastal water causes problems with the atmospheric corrections, as does absorption from non-algal particles. Wetting and drying of tidal flats in Cobequid Bay and Windsor Bay can lead to uncertainty and systematic errors in satellite estimates of TSM concentration. Parker *et al.,* (2007) documented the extensive areas of intertidal mud flats in Minas Basin, owing to the high tidal range, coastal erosion and sediment washed in from the Salmon, Cornwallis, and Avon rivers. These areas either underlie or fringe the locations in the maps of satellite-derived TSM concentration that show limited or no annual cycle, suggesting that the satellite may not be able to resolve changes in TSM in these areas. Furthermore, the distinguishing of the seabed at low tide from TSM-rich water at high tide is difficult over the shallow regions of Minas Basin.

Sediment concentrations may be too high for accurate estimation by the MERIS algorithm. Based on the Crewe's *in situ* measurements (Crewe, 2004), the surficial mean

suspended sediment concentration is approximately 50 g/m^3 during the whole summer at the head of Salmon River Estuary. Concentrations of this magnitude are at the upper limit that can be resolved by MERIS (Shen *et al*., 2010a). Concentrations of more than 150 g/m^3 have been observed at the head of Cobequid Bay in the eastern portions of the Minas Basin (Parker *et al.*, 2007). Interestingly, the mean of satellite TSM concentration at the head of Cobequid Bay was below 10 g/m^3 during the summer (Figure 16). Similarly, recorded surficial TSM concentration greater than 100 g/m^3 has been observed near the mouth of the Cornwallis River in the Southern Bight, but such large concentrations do not exist in this area according to the satellite-derived data (Parker *et al.,* 2007). These differences suggest that MERIS consistently underestimates TSM concentration in shallow water where sediment concentrations are large. Such underestimation may explain why the model predicts greater seasonal variability over tidal flats than the satellite TSM show. Unfortunately, there were no data to evaluate the MERIS TSM data in winter at Cobequid Bay.

It should be noted finally that MERIS might work reasonably well in Minas Basin because inorganic sediment concentrations are so high. The suspended inorganic matter reflects light to a much greater extent than other substances.

4.2.2 Accuracy of Delft3D TSM Concentration

The model may be inaccurate in the shallow areas. The model predictions may be inaccurate in shallow areas because initial conditions were formulated improperly; some physical processes were not considered, or bathymetry was inaccurate.

Comparison between ADCP observed currents (speed and velocity components) with Delft3D model predictions at site A5 show that model results at this site agree well with the observed tidal amplitudes and phases (Figure 20). Delft3D hydrodynamics results also compared well with the FVCOM model results after comparing with the results of Wu. Both models predict a non-uniform distribution of currents across Minas Passage

during the ebb tide and strong horizontal current shear with re-circulation during the flood stage of the tidal cycle (Wu *et al.*, 2011).

In Minas Basin, the model shows that the fine suspended sediment concentration and the distribution of mud on the surface are controlled by a combination of the sediment parameters and the physical processes the cause re-suspension and transport. The distribution of sediment on the bed for the initial condition is highly simplified in that it treats the bottom either as mud-covered or bare. The effect of sand re-suspension over the shallow flats is neglected. Consideration of sand could enhance rather than reduce seasonal differences in the model output due to increased re-suspension of sand by waves during more energetic winter months. Delft3D-FLOW may not predict TSM concentration over shallow areas because in this study it did not include some processes that re-suspend sediment. Perhaps most importantly, the model did not include waves, which are important for re-suspending sediment in shallow water. In the intertidal zone of Minas Basin, wave activity on the tidal flats is very important in creating turbid conditions that characterize the Cobequid Bay and Windsor Bay (Parker *et al*., 2007). Inclusion of waves would enhance rather than reduce seasonal differences in modelled TSM concentration. Another question is whether the model bathymetry of Minas Basin is accurate. The suspended sediment sources are the shallow areas of Cobequid Bay and Windsor Bay where bathymetry is dynamic and poorly resolved. Inaccurate bathymetry can degrade model predictions (Figure 22), but it is unlikely any inaccuracies would introduce seasonal bias into model results.

4.2.3 Accuracy of Comparison

The differences between model and satellite TSM concentration patterns might be caused by the time averaging technique. As mentioned before, the seasonal mean of the satellite TSM concentrations were derived from the time averaging of two months of satellite data, but the mean of the model TSM was obtained by averaging of three days model output. MERIS satellite overpasses the study area daily, and the model simulated the TSM hourly. Although the time averaging technique may induce magnitude

differences, it should not influence the TSM concentration distribution or variation in the entire Basin or produce an artificial seasonal signal over shallow areas. Additionally, the timing within the tidal cycle also causes a bias in the MERIS results.

The differences between model and satellite TSM concentration pattern might be caused by portion of the water column measured. The vertical resolution of Delft3D model is variable in Minas Basin, so the layer thickness at the surface varied between locations. The surface layer thickness varied from 1 to 12 m. However, the portion of the water column MERIS measured is based on the path of photons through the water column. The geometrical thickness of the vertical water layer from which 90% of the remotely sensed ocean colour signal comes from can be approximated by the vertical attenuation coefficient for downward irradiance, so the geometrical thickness of water column is determined according to the concentrations and inherent optical properties of water substances (MERIS product handbook, 2002). The satellite-derived TSM in Minas Basin derives from a thin surficial layer of the water column, and it does not include deeper layers that contribute to the model estimate of surficial TSM concentration. In short, the optical depth of the satellite is shallower than the model's surface layer.

It was found that the observed annual cycle of TSM in the centre of Minas Basin is real, but the lack of an annual cycle in satellite-derived TSM over shallow areas is questionable. Model simplifications and inaccuracies are unlikely to produce a spurious seasonal difference between summer and winter simulations. In fact, omitted processes like waves and sand transport are likely to enhance rather than limit the seasonal differences predicted by the model.

CHAPTER 5 CONCLUSION AND RECOMMENDATIONS

5.1 Summary of Scientific Results

Ocean colour data from the satellite-based MERIS sensor was used to determine the spatial distribution of suspended sediment in the macro-tidal coastal embayment of Minas Basin. During this research, several results have emerged. The mean values of TSM concentration over 1 km^2 pixel boxes derived from MERIS data indicate a strong annual change in most areas of Minas Basin. Larger TSM concentrations are observed in late-winter (February and March), and smaller TSM concentrations characterize late-summer (July and August). Additionally, the peak of TSM concentration in winter varies over the Basin, which is reduced both westward and northward. At Cobequid Bay, the TSM concentrations are always higher than other areas and lack seasonal patterns of variability. In the central Minas Basin and Cobequid Bay, the TSM magnitude varies from 15 to 45 g/m^3 in winter and is below 20 g/m^3 in summer. Temporal autocorrelation analysis was carried out with TSM time series throughout the Basin. The strength of annual signal varies throughout the Basin, with the largest variation occurring in the middle of Minas Basin, and the smallest variation occurring in Cobequid Bay, near Windsor Bay and along the boundaries of the Basin. In this study, data were not collected to explain why the TSM concentration showed seasonal variability. There are some reasonable mechanisms, such as biofilm control of sediment erosion rate. Comparison of satellite-derived TSM concentration and *in situ* measurements at different sites in Minas Basin indicates that *in situ* surficial TSM concentration measurements are higher than satellite observations in Minas Basin, but they have similar magnitude and variation.

Satellite-derived TSM concentrations were compared with TSM derived from the three-dimensional Delft3D-FLOW model. Delft3D results at site A5 agree qualitatively well with the observed tidal amplitudes and phases. A range of sediment parameters was tested in the Delft3D model to derive values that were best able to reproduce the summer and winter concentrations of TSM in Minas Basin. Quantitative comparisons between model and satellite-derived TSM during the summer and winter showed similar

magnitudes and spatial distributions, except over shallow regions fringing the central Basin. The Delft3D model over-predicts TSM concentration relative to satellite-derived estimates in the shallow areas in winter and under-predicts TSM in shallow areas in summer. The source of the discrepancies in shallow water may be due to model assumptions or initial conditions, but it more likely arises from inaccurate retrieval of TSM concentration by the satellite in these regions. The modelling approach was idealized: to vary the sediment parameters in each run and keep the hydrodynamic conditions the same. They vary widely in space and time and a perfect match between model and data will be very difficult to achieve in all parts of the basin without a significant amount of field observations to define input and initial conditions.

5.2 Recommendations

As follow up to this study, there are recommendations for future research in combining remote sensing and Delft3D to analyze sediment dynamics in Minas Basin.

1. The accuracy of the MERIS TSM algorithm should be assessed for higher (over 50 g/m^3) concentrations.

2. More *in situ* data are required for assessing the accuracy of satellite-derived TSM concentration.

3. To improve the accuracy of the Delft3D simulation, the distribution of bed sediments should be measured in the field. The model should incorporate key processes that influence the surficial suspended sediment concentration in high turbidity water, specifically wind and waves. Increasing accuracy of bathymetry in Minas Basin will improve the Delft3D ability to predict TSM concentration accurately over the shallow areas.

4. Arguably the most important next step is examining how the biological activity on the bottom of the seabed affects on the dynamics of cohesive sediment on large spatial and temporal scales in Minas Basin. Model parameterization of erosion rate should be based on *in situ* measurements of biofilms and erosion rates collected throughout the year in Minas Basin.

BIBLIOGRAPHY

Amos, C. L., Joice, G. H. E., The Sediment Budget of the Minas Basin, Bay of Fundy, N.S., Bedford Institute of Oceanography, Data Series Bl-D-77-3, 1977.

Amos, C. L., The determination of suspended sediment concentration in a macrotidal system using Landsat Data, *Journal of sedimentary petrology*, Vol. 49, No.1, p. 0159-0174, 1979.

Amos, C., Mosher, D., Erosion and deposition of fine-grained sediments from the Bay of Fundy, *Sedimentology*, 32, 815-832, 1985.

ATBD Chapter 2.12, The algorithm theoretical basis documents of the MERIS Level 2, GKSS Research Centre, ESA.

Bourg, L., Delwart, S., Huot, J. P., Rast, A., Calibration and early results of MERIS on ENVISAT, in IEEE International Geoscience and Remote Sensing Symposium (IGARSS 2002)/24th Canadian Symposium on Remote Sensing, Toronto, Canada, pp. 599-601, 2002.

Borsje, B., Biological influence on sediment transport and bed composition for the Western Wadden Sea, Master essay, University of Twente, 104 p., 2006.

Bugden, G., Milligan, T., Law, B., The Distribution of Suspended Particulate Matter in Northumberland Strait, in Atlantic Canada Coastal and Estuarine Science Society Annual Meeting, Cape Breton University, 2007.

Crewe, B., Characterization of sediment in the Salmon River Estuary, Master essay, Dalhousie University, 126 p., 2004.

Daborn, G. R., Zooplankton Studies in the Upper Bay of Fundy Since 1976: Update on the Environmental Consequences of Tidal Power in the Upper Reaches of the Bay of Fundy, University of Moncton, NB (Canada), 8 November 1982, Moncton, NB, 1984.

Dadswell, M. J., Rulifson, R. A., Daborn, G. R., Potential Impact of Large-Scale Tidal Power Developments in the Upper Bay of Fundy on Fisheries Resources of the Northwest Atlantic. *Fisheries*, 11, 26-35, 1986.

Dalrymple, R. W., Knight, R. J., Zaitlin, B. A., Middleton, G. V., Dynamics and facies model of a macro-tidal sand-bar complex, Cobequid Bay-Salmon River Estuary (Bay of Fundy), *Sedimentology*, 37, 577-612, 1990.

Diggle, P. J., Time series: A Biostatistical Introduction, Oxford Statistical Science Series 5, Oxford University Press, 1990.

Doerffer, R., Schiller H., The MERIS Case 2 water algorithm, *International Journal of Remote Sensing*, Vol.28, Nos. 3-4, 517-535 Feburary 2007.

Dupont, F., Hannah, C. G., Greenberg, D., Modelling the Sea Level in the Upper Bay of Fundy, *Atmosphere-Ocean*, 43(1), 33-47, 2005.

European Space Agency, MERIS product handbook, from http://envisat.esa.int/envisat/dataproducts/, 2002.

ESA website: http://envisat.esa.int/instruments/meris/data-app/dataprod.html#prod-struct

Fader, G. B. J., King, L. H., MacLean, B., Surficial geology of the eastern Gulf of Maine and the Bay of Fundy, *Geological Survey of Canada*, paper 76-17, 23 p., 1977.

Gray, J. R., Gartner, J. W., Technological advances in suspended-sediment surrogate monitoring, *Water Resources Research*, Volume 45, Issue 4, 2009.

Greenberg, D. A., Amos, C. L., Suspended sediment transport and deposition modeling in-the Bay of Fundy, Nova Scotia - a region of potential tidal power development, *Canadian Journal of Fisheries and Aquatic Sciences*, 40(Suppl. 1): 20 – 34, 1983.

Hill, P. S., Milligan, T. G., Geyer, W. R., Controls on effective settling velocity of suspended sediment in the Eel River flood plume, *Continental Shelf Research*, 20, 2095-2111, 2000.

Kritikos, H., Yorinks, L., Smith, H., Suspended solids analysis using ERTSA data, *Remote Sensing of Environment*, 3: 69-80,1974.

Knight, R. J., Sediments, Bedforms and Hydraulics in a Macrotidal Environment, Cobequid Bay (Bay of Fundy), Nova Scotia, Unpublished PhD thesis, McMaster University, Hamilton, ON, 693 pp., 1977.

Lesser, G. R., Roelvink J. A., Van Kester, J. A. T. M., Stelling, G. S., Lakhan, V., Development and validation of a three-dimensional morphological model, *Coastal Engineering*, Vol. 51, 883-915, 2004.

Li, M. Z., Hannah, C., Perrie, W., Tang, C., Prescott, R., Greenberg, D.A., Numerical model predictions of seabed shear stress, sediment mobility and sediment transport in the Bay of Fundy. Abstract with program, Atlantic Geoscience Society (AGS) Colloquium 2010, 5–6 February 2010, Wolfville, Nova Scotia, 2010.

Mikkelsen, O. A., Milligan, T. G., Hill, P. S., Moffatt, D., INSSECT-an instrumented platform for investigating floc properties close to the seabed, *Limnology and Oceanography: methods*, 226-236, 2004.

Miller, R. L., Liu, C., Buonassissi, C. J., Wu, A., A Multi-Sensor Approach to Examining the Distribution of Total Suspended Matter (TSM) in the Albemarle-Pamlico Estuarine System, NC, USA, *Romote Sensing*, 3, 926-973, 2011.

Munday, J. C., Alfoldi, T. T., Amos, C. L., Bay of Fundy verification o1 a system for multidate Landsat measurement of suspended sediment, *Satellite Hydrology*, pp. 620-640, 1979.

Parker, M., Westhead, M., Service, A., Ecosystem Overview Report for the Minas Basin, Nova Scotia, *Oceans and Habitat Report*, 2007.

Ruddick, K., Park, Y., Nechad, B., MERIS imagery of Belgian coastal waters: mapping of suspended particulate matter and chlorophyll-a, Proc. MERIS User Workshop, Frascati, Italy, 10-13 November, 2003.

Shen, F., Verhoef, W., Zhou, Y. X., Salama, Mhd.S., Liu, X.L., Satellite estimates of wide-range suspended sediment concentrations in Changjiang (Yangtze) estuary using MERIS data, *Estuaries and Coasts*, doi: 10.1007/s12237-010-9313-2, 2010a.

Shen, F., Salama, M. S., Zhou, Y. X., Li, J.F., Su, Z., Kuang, D. B., Remote-sensing reflectance characteristics of highly turbid estuarine waters – a comparative experiment of the Yangtze River and the Yellow River, *International Journal of remote sensing*, 31(10), 2639–2654, 2010b.

Smith, P., Interim report: impacts of tidal energy extraction on sediment dynamics in Minas Basin, Bay of Fundy, NS, 2011.

Stea, R., A Virtual Fieldtrip of the Landscapes of Nova Scotia, Nova Scotia Department of Natural Resources, NS, 2003.

Stow, C. A., Jolliff, J., McGillicuddy, J. D. J., Doney, S. C., Allen, J. I., Friedrichs, M. A. M., Rose, K. A., Wallhead, P., Skill assessment for coupled biological/physical models of marine systems, *Journal of Marine Systems*, 76, 4-15, 2009.

Sutherland, J., Walstra, D. J. R., Chesher, T. J., van Rijn, L. C., Southgate, H. N., Evaluation of coastal area modelling systems at an estuary mouth, *Coastal Engineering*, Vol. 51, 119-142, 2004.

Tang, S., Dong, Q., Chen, C., Liu, F., Jin, G., Retrieval of suspended sediment concentration in the Pearl River Estuary from MERIS using support vector machines. Geoscience and Remote Sensing Symposium, IEEE International, IGARSS, 2009.

Taylor, K.E., Summarizing multiple aspects of model performance in a single diagram. *Journal of Geophysical Research*, 106(D7): 7183–7192, 2011.

Thomas, M. L. H., Intertidal Resources of the Bay of Fundy, Fundy Tidal Power and the Environment, Acadia University, Wolfville, NS, 1976.

Van Proosdij, Milligan, T., Bugden, G., Butler, K., A Tale of Two Macro Tidal Estuaries: Differential Morphodynamic Response of the Intertidal Zone to Causeway Construction, *Journal of Coastal Research*, Special Issue 56, 2009.

Wu, Y., Chaffey, J., Greenberg, D. A., Colbo, K., Smith, P. C., Tidally-induced sediment transport patterns in the upper Bay of Fundy: A numerical study, *Continental Shelf Research,* 31, 2041-2053, 2011.

Winterwerp, J.C., On the flocculation and settling velocity of estuarine mud, *Continental Shelf Research*, 22, pp. 1339-1360, 2002.

WL|Delft Hydraulics, "User Manual Delft3D-FLOW". WL|Delft Hydraulics, Delft, 2006.

Zhang, Y., Lin, S., Lin, J., Qian, X., Ge, Y., Time-series MODIS Image-based Retrieval and Distribution Analysis of Total Suspended Matter Concentrations in Lake Taihu (China), *International Journal of Environmental Research and Publish Health*, 7, 3545-3560, 2010.

APPENDIX A MERIS Spectral Bands and Applications

No.	Band centre (nm)	Band width (nm)	Applications
1	412.5	10	Yellow substance and detrital pigments
2	442.5	10	Chlorophyll absorption maximum
3	490	10	Chlorophyll and other pigments
4	510	10	Suspended sediment, red tides
5	560	10	Chlorophyll absorption minimum
6	620	10	Suspended sediment
7	665	10	Chlorophyll absorption & fluorescence reference
8	681.25	7.5	Chlorophyll fluorescence peak
9	708.75	10	Fluorescence reference, atmosphere corrections
10	753.75	7.5	Vegetation, cloud, O_2 absorption band reference
11	760.625	3.75	O_2 R- branch absorption band
12	778.75	15	Atmosphere corrections
13	865	20	Atmosphere corrections
14	885	10	Vegetation, water vapour reference
15	900	10	Water vapour

APPENDIX B Delft3D Mean TSM Concentration in Minas Basin

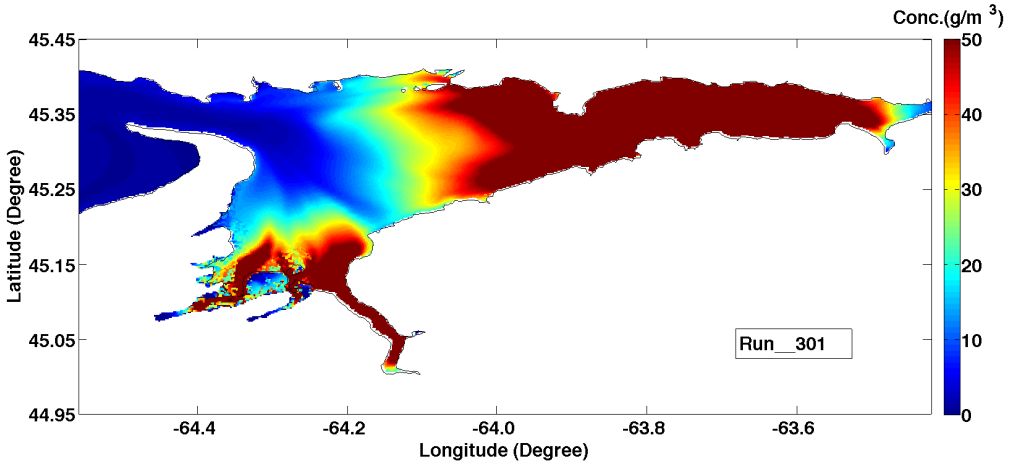

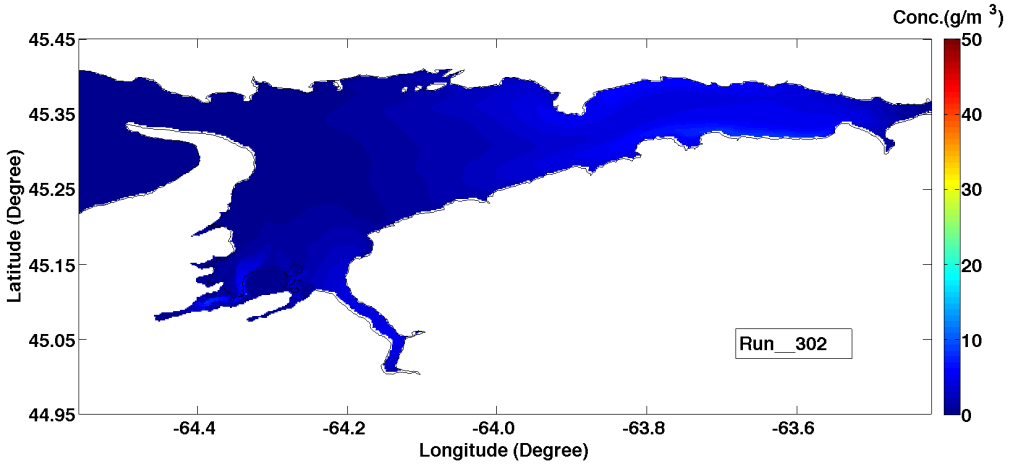

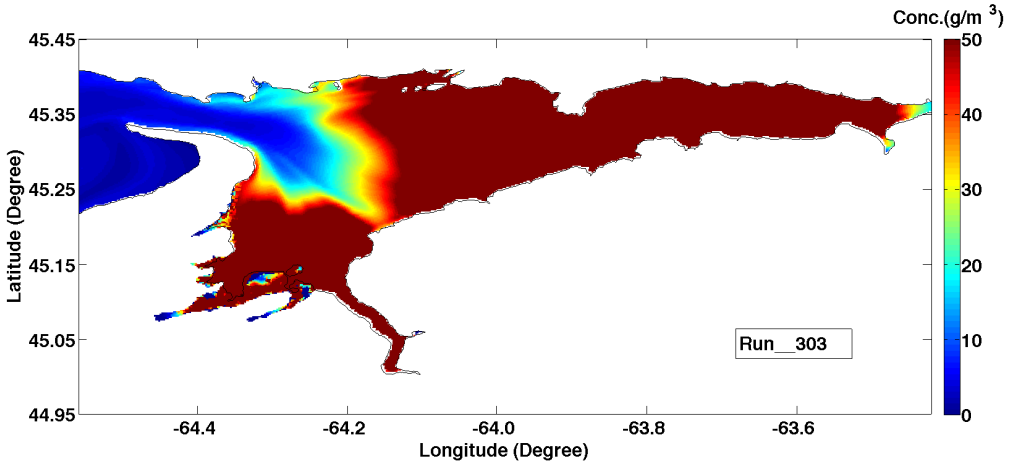

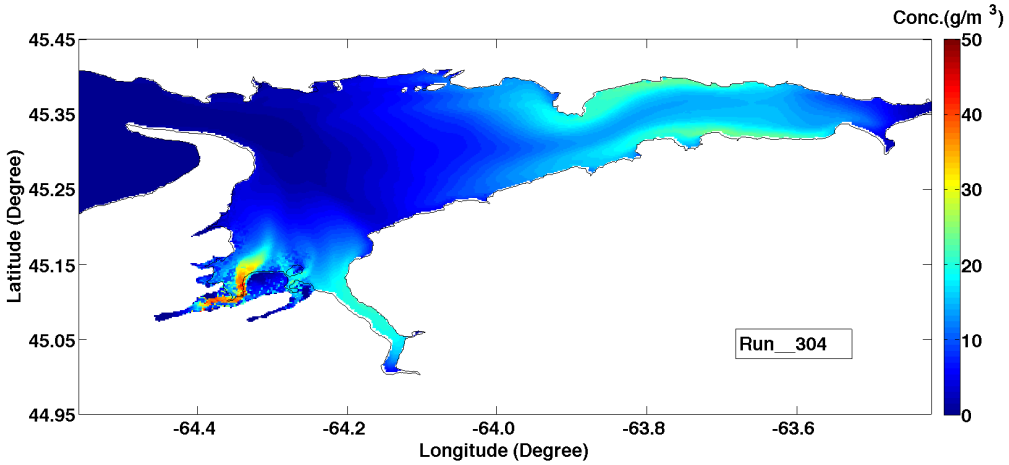
Conc.(g/m 3)
50
40
30
20
10
0
45.45
45.35
45.25
45.15
45.05
44.95
Latitude (Degree)
-64.4
-64.2
-64.0
-63.8
-63.6
Longitude (Degree)
Run__304

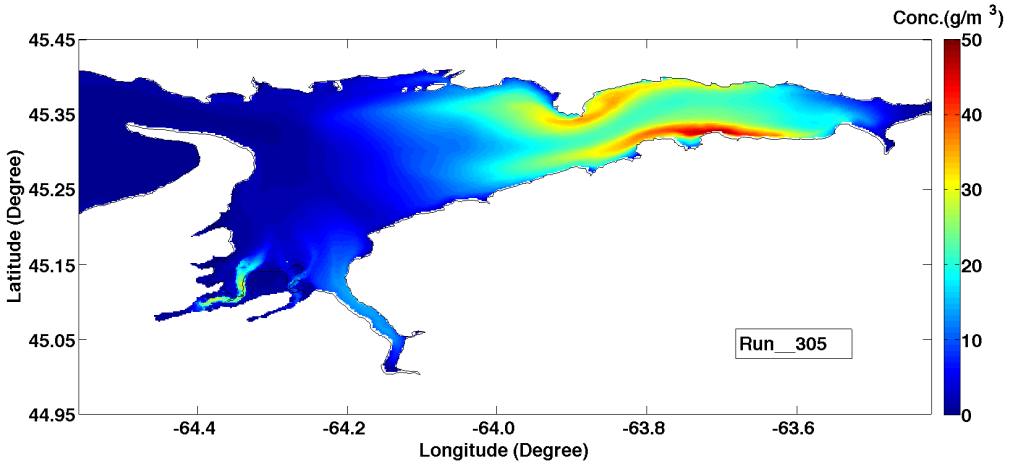
Conc.(g/m 3)
50
40
30
20
10
0
45.45
45.35
45.25
45.15
45.05
44.95
Latitude (Degree)
-64.4
-64.2
-64.0
-63.8
-63.6
Longitude (Degree)
Run__305

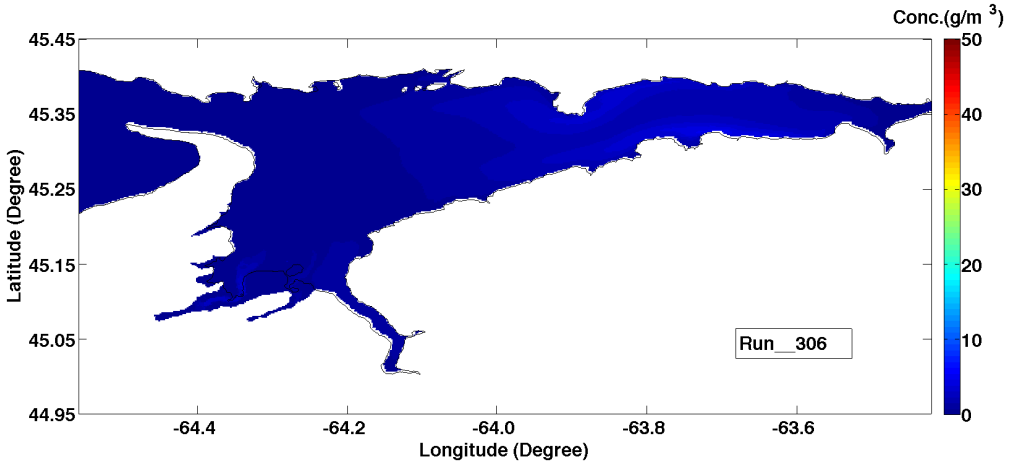
Conc.(g/m 3)
50
40
30
20
10
0
45.45
45.35
45.25
45.15
45.05
44.95
Latitude (Degree)
-64.4
-64.2
-64.0
-63.8
-63.6
Longitude (Degree)
Run__306

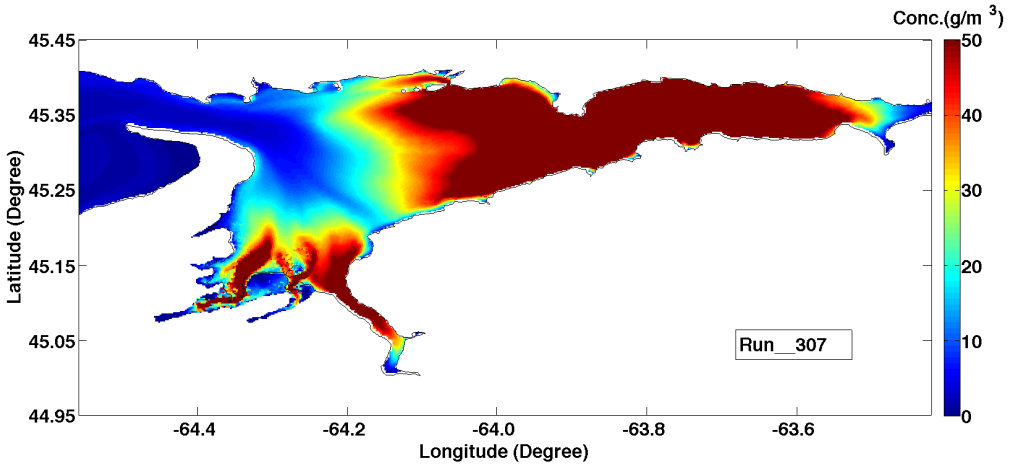
Conc.(g/m 3)
45.45
45.35
45.25
45.15
45.05
44.95
Latitude (Degree)
-64.4
-64.2
-64.0
-63.8
-63.6
Longitude (Degree)
50
40
30
20
10
0
Run__307

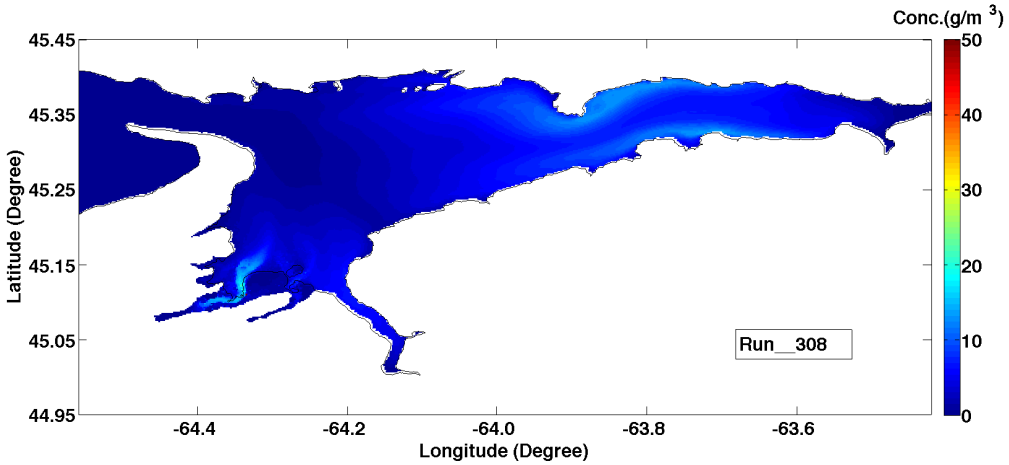
Conc.(g/m 3)
45.45
45.35
45.25
45.15
45.05
44.95
Latitude (Degree)
-64.4
-64.2
-64.0
-63.8
-63.6
Longitude (Degree)
50
40
30
20
10
0
Run__308

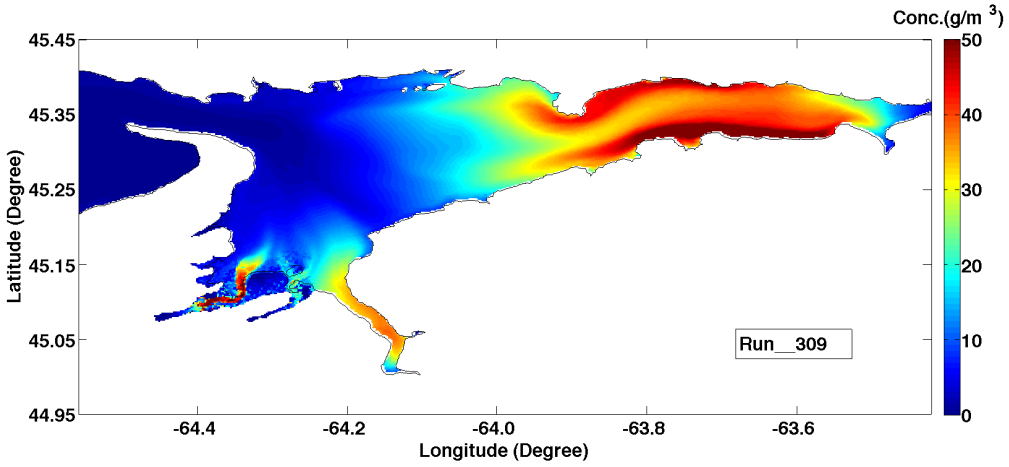
Conc.(g/m 3)
45.45
45.35
45.25
45.15
45.05
44.95
Latitude (Degree)
-64.4
-64.2
-64.0
-63.8
-63.6
Longitude (Degree)
50
40
30
20
10
0
Run__309

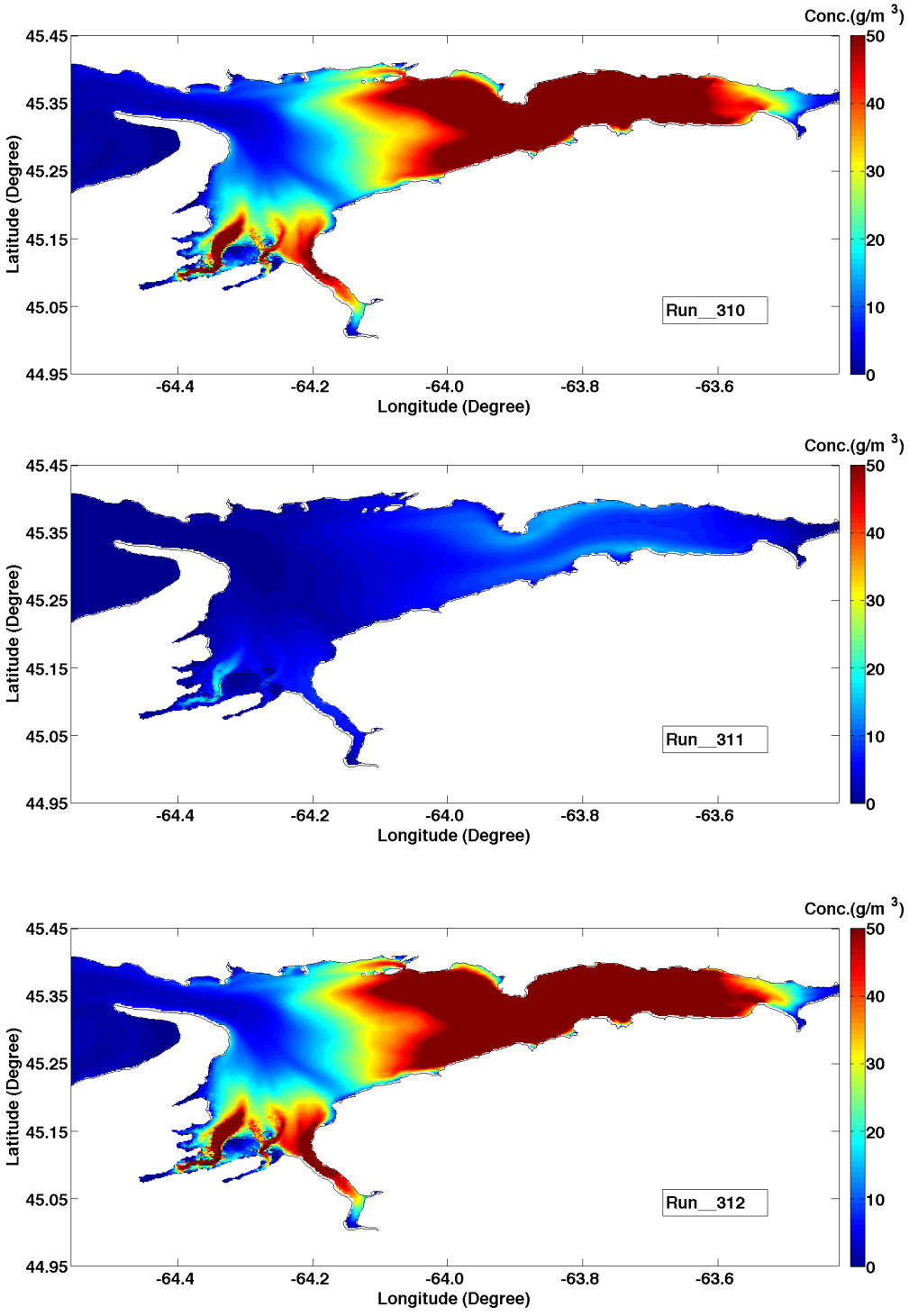

Figures B1-B12: Delft3D model suspended surficial mud concentrations for each run in Minas Basin.

APPENDIX C Satellite and Model Comparisons

Run_301:

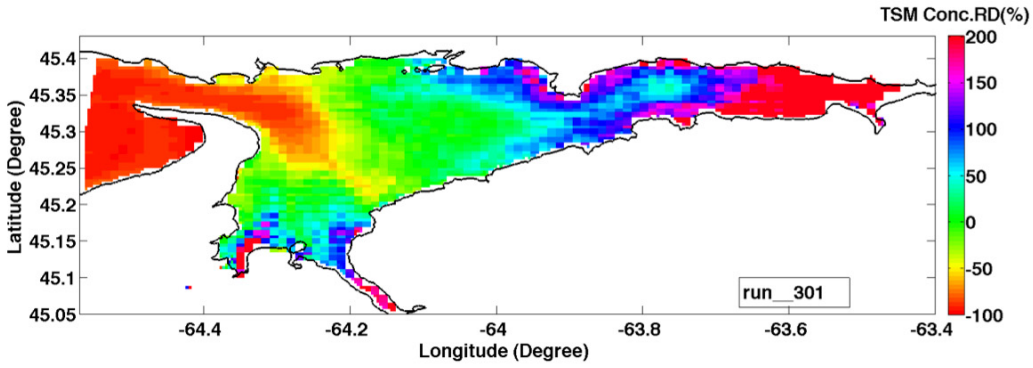

Run_303:

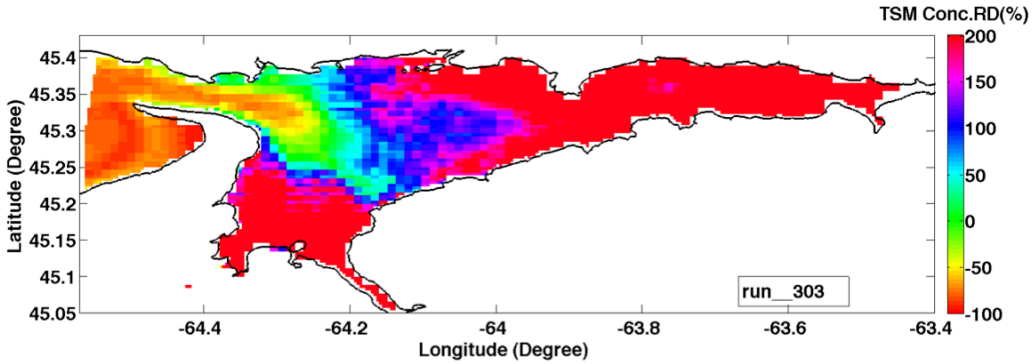

Run_305:

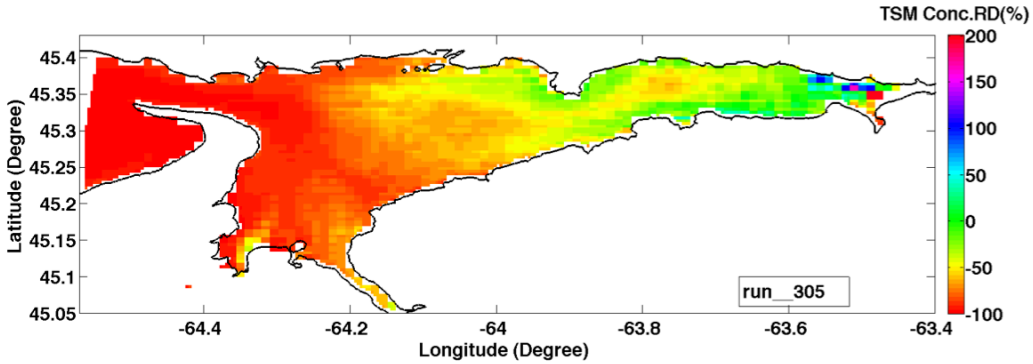

Run_307:

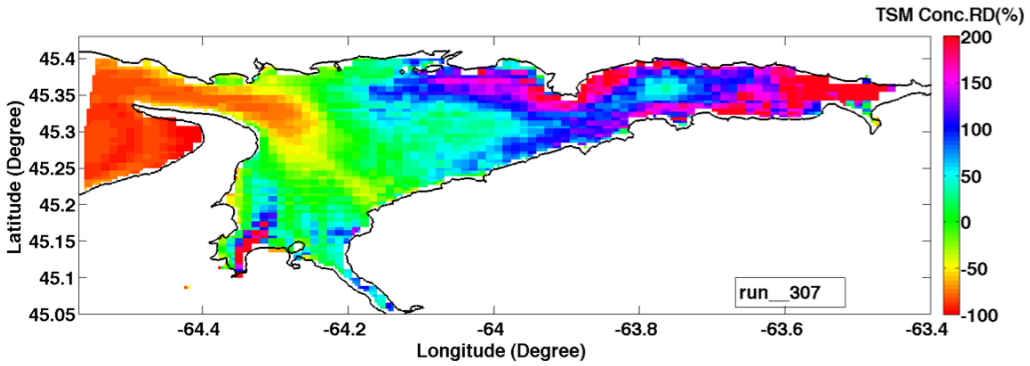

Run_309:

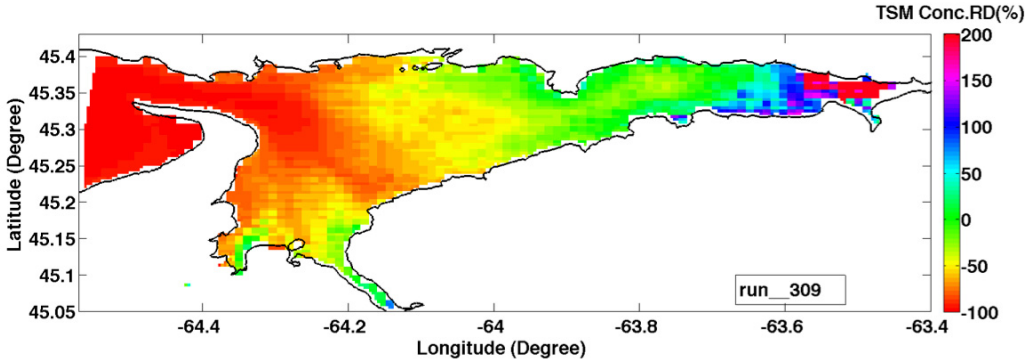

Run_310:

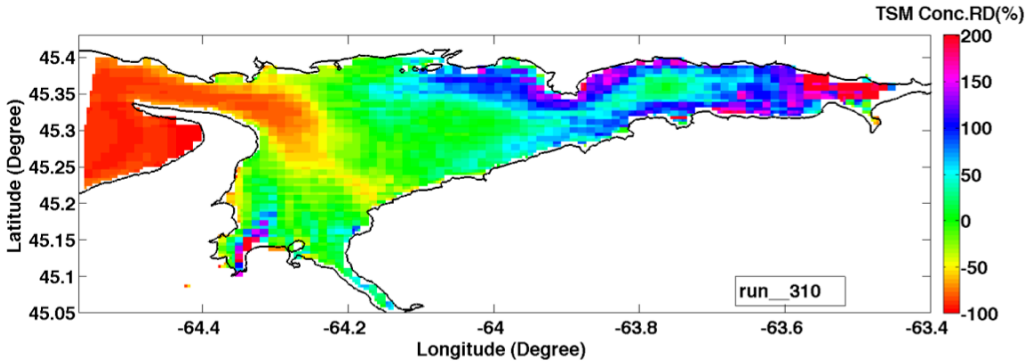

Run_312:

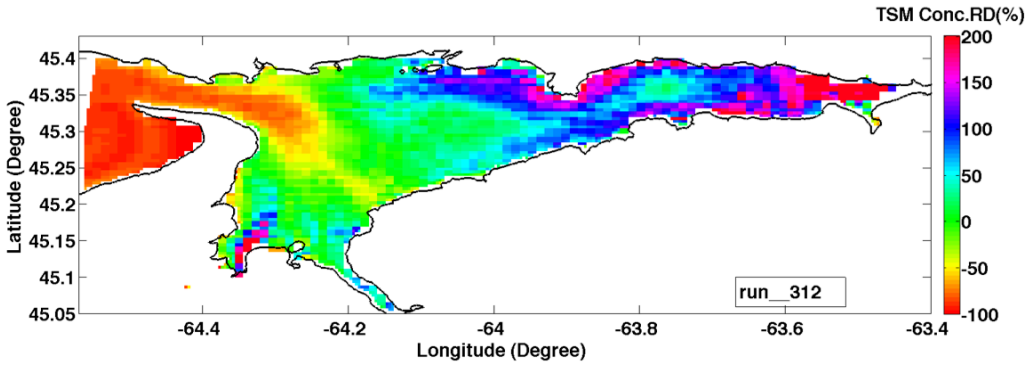

Figures C1-C7: Quantitative comparisons between Delft3D Model and MERIS satellite TSM concentration during winter 2009.

Run_302:

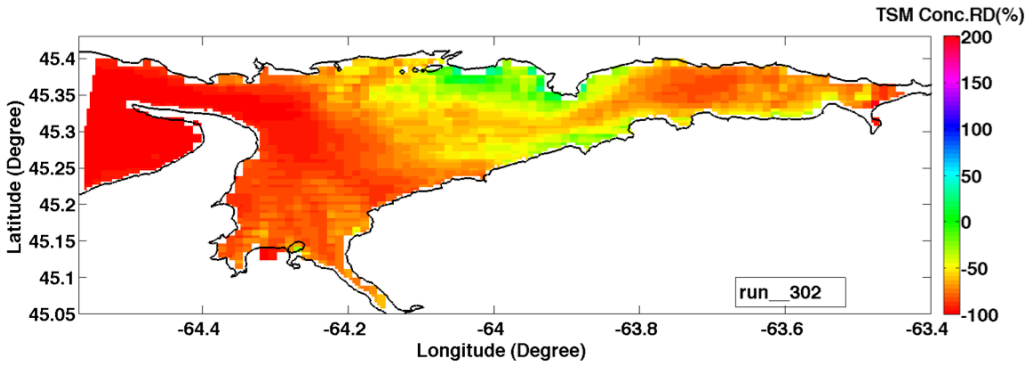

Run_304:

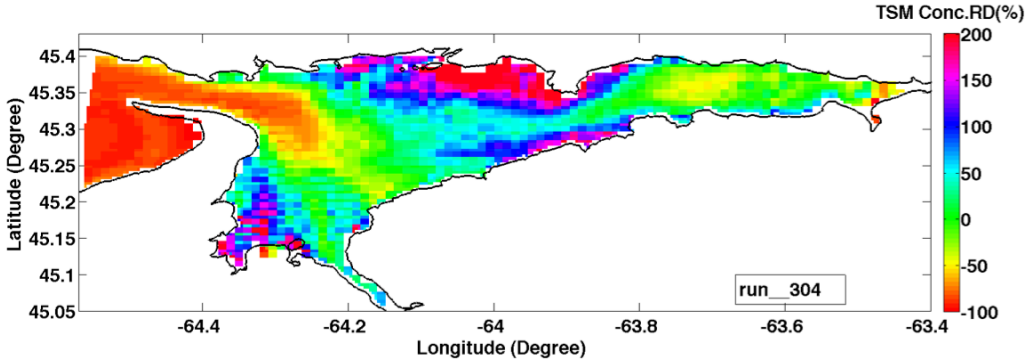

Run_305

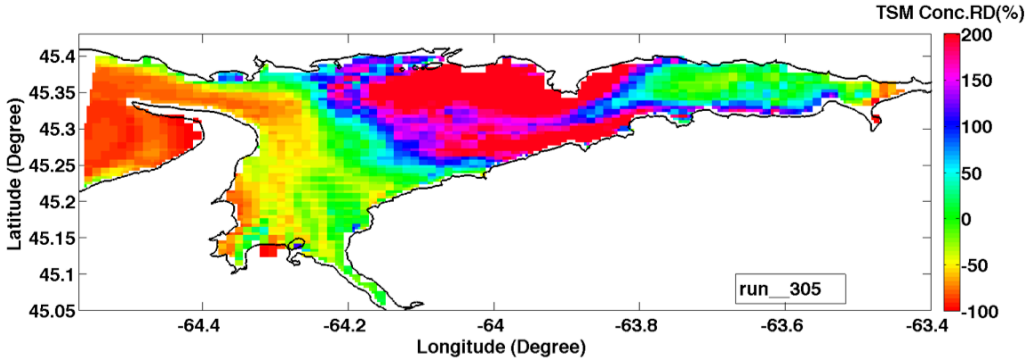

Run_306:

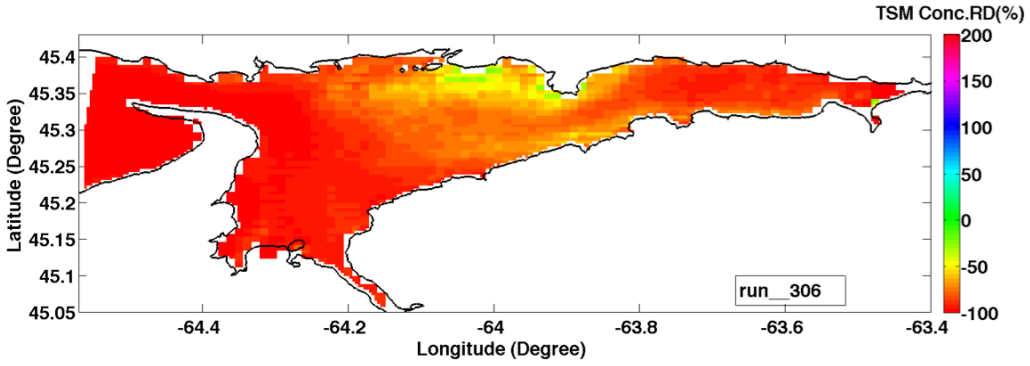

Run_308:

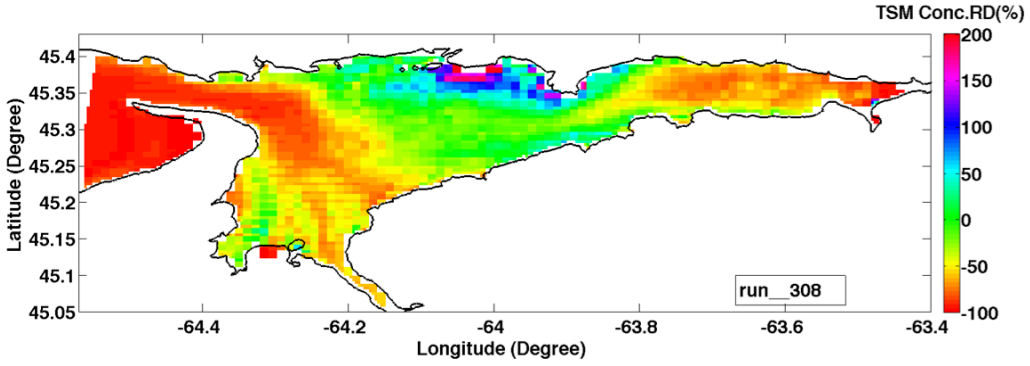

Run_311:

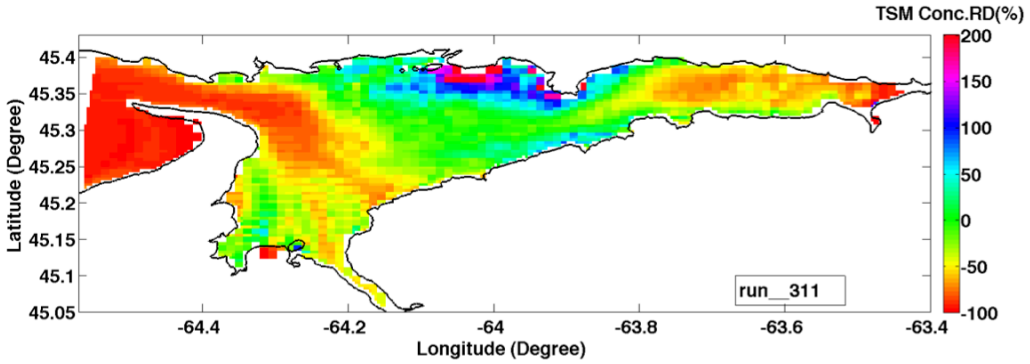

Figures C8-C13: Quantitative comparisons between Delft3D Model and MERIS satellite TSM concentration during summer 2010.